DELHI TECHNOLOGICAL UNIVERSITY

(Formerly Delhi College of Engineering)

Shahbad Daulatpur, Bawana Road,

Delhi-110042

ANALYSIS AND OPTIMIZATION OF CONNECTIN FIBER REINFORCED PLASTIC

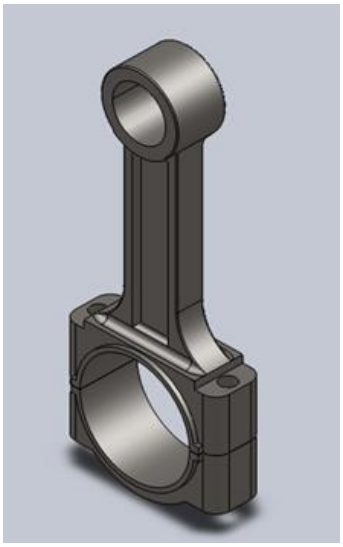

Submitted by
Amit Rawal
2K13/PIE/27
M-Tech Production (Part Time)

DELHI TECHNOLOGICAL UNIVERSITY

(Formerly Delhi College of Engineering)

Shahbad Daulatpur, Bawana Road,

Delhi-110042

CERTIFICATE

This is to certify that this thesis report entitled, **"ANALYSIS AND OPTIMIZATION OF CONNECTING ROD USING FIBER REINFORCED PLASTIC"** being submitted by **Amit Rawal (Roll No. 2K13/PIE/27)** at Delhi Technological University, Delhi for the award of the Degree of Master of Technology as per academic curriculum. It is a record of bonafide research work carried out by the student under my supervision and guidance, towards partial fulfillment of the requirement for the award of Master of Technology degree in Production Engineering. The work is original as it has not been submitted earlier in part or full for any purpose before.

Mr.Vijay Gautam
Assistant Professor
Department of Mechanical Engineering
Delhi Technological University
Delhi-110042

DELHI TECHNOLOGICAL UNIVERSITY

(Formerly Delhi College of Engineering)

Shahbad Daulatpur, Bawana Road,

Delhi-110042

STUDENT'S DECLARATION

I, **Amit Rawal (Roll No. 2K13/PIE/27),** hereby certify that the work which is being presented in this thesis entitled **"ANALYSIS AND OPTIMIZATION OF CONNECTING ROD USING FIBER REINFORCED PLASTIC"** is submitted in the partial fulfillment of the requirement for degree of **Master of Technology (Production & Industrial Engineering)** in Department of Mechanical Engineering at **Delhi Technological University** is an authentic record of my own work carried out under the supervision of **Mr. Vijay Gautam (Assistant Professor), Dr. Pravin Kumar (Assistant professor) and Mr. Saurabh Agarwal (Assistant Professor).** The matter presented in this thesis has not been submitted in any other University/Institute for the award of Master of Technology Degree. Also, it has not been directly copied from any source without giving its proper reference.

Signature of Student

This is to certify that the above statement made by the candidate is correct to the best of my knowledge.

Signature of Supervisor

Signature of HOD

Signature of External Examiner

DELHI TECHNOLOGICAL UNIVERSITY

(Formerly Delhi College of Engineering)

Shahbad Daulatpur, Bawana Road,

Delhi-110042

ACKNOWLEDGEMENT

I express my deepest sense of gratitude to **Shri Vijay Gautam**, Department Of Mechanical Engineering, DTU for his keen interest, encouragement, constructive suggestions and esteemed guidance throughout the project.

I would like to thank **Shri Amit Pal** for his valuable advices, encouragement and allowing us to use the facilities of I.C Engine lab. I really thank him for providing us with such a conductive environment for experimenting and his energetic cooperation.

We wish to thank all the faculty members & staffs of Department of Mechanical Engineering for their support and help during the project.

Last but far from least; I would like to express my heart-felt thanks to my parents for their endless support, without which I could not have completed my work. I would also like to thank my friends for their persistent bugging and challenges they put forward to us to complete this effort.

DELHI TECHNOLOGICAL UNIVERSITY

(Formerly Delhi College of Engineering)

Shahbad Daulatpur, Bawana Road,

Delhi-110042

Abstract

Connecting rod is an important dynamic link rod between piston and crank shaft. This undergoes a complex state of stress during working and adds to the problem in design for strength. Mostly connecting rods are manufactured using carbon steel and in recent days composite materials are finding its application in connecting rod. In the present paper a finite element model was developed to study the effects of various stress patterns on the design of the rod. To achieve the objective, connecting rod is modelled by taking the dimensions from actual component captured from a blue light scanner. The practical load-data points as a function of crank angle are directly collected from the four cylinder diesel engine. Simulation software is used to determine the pressure in the cylinder. The values of angular velocity and acceleration are calculated theoretically using analytical equations. Using the above data, static and dynamic finite element simulation is carried out successfully and connecting rod is replaced by carbon based composite material reinforced with silicon carbide. And it describes the modelling and analysis of connecting rod. Finite Element Analysis was carried out by considering two materials. The parameter like von misses stress, von misses strain and displacement was obtained from Abacus software. Over the past years, improvements in performance efficiency have been achieved by simplifying the design of the structural components and using composite materials to reduce the overall weight.

Keywords: Connecting rod, finite element analysis, Design for strength, Crank angle, Angular velocity, Angular acceleration.

List of contents

List of Figure

List of Table

Nomenclature

aA, aP	Acceleration of point A, piston
a	Absolute acceleration of a point on the connecting rod
ac.gX, ac.gY	X, Y components of the acceleration of the C.G. of the connecting rod
E	Modulus of elasticity
e	Offset, the distance from the centerline of the slider path to the crank bearing.
FI, FS	Failure index, factor of safety
Fa	Load amplitude
Fm	Mean load
FX	Force in X direction on piston
FAX, FAY	X, Y components of the reactions at the crank end
FBX, FBY	X, Y components of the reactions at the piston pin end
IZZ	Moment of Inertia about Z axis and C.G. of the connecting
m	Slope of the modified Goodman line
mp, mc	Mass of piston assembly, connecting rod
p	Normal pressure
po	Normal pressure constant
Pt, Pc	Tensile, compressive resultant load in the direction of the rod length
r	Transition radius
R	Radius of crankshaft pin
r1	Radius of crank

r2	Connecting rod length
r3	Distance from crankshaft bearing center to slider (piston pin center)
ro	Outer radius of outer member
ri	Inner radius of inner member
Sa, Sm	Alternating, mean stress
Sax, Say, Saz	Alternating x, y, z stress
Smx, Smy, Smz	Mean x, y, z stress
Smax, Smin	Maximum, minimum stress
SNf	Equivalent stress amplitude at R = -1
Sqa, Sqm	Equivalent stress amplitude, equivalent mean stress
Su	Ultimate tensile strength
t	Thickness of the connecting rod at the loading surface
u	Distance of C.G. of the connecting rod from crank end center
Vp	Slider velocity in X direction
Δ	Total radial interference
P	Position vector of any point on connecting rod
β	Connecting rod angle with positive direction of X axis
η	$(2\pi-\beta)$
$\omega 1$	Angular velocity of crankshaft
$\omega 2$	Angular velocity of connecting rod
$\alpha 2$	Angular acceleration of connecting rod

1. Introduction

1.1 Background

Connecting rods (CR) is a dynamic machine component widely used in variety of internal combustion engines. It is used to transmit thrust of the piston to the crankshaft resulting in rotational motion of the crankshaft. It consists of a pin-end, a shank section, and a crank-end. Pin-end and crank-end pin holes are machined to permit accurate fitting of bearings. One end of the CR is connected to the piston by the piston pin. The other end revolves with the crankshaft and is split to permit it to be clamped around the crankshaft. This split type of big end of the CRs are preferred for the multi-cylinder engines. In a reciprocating piston engine, the connecting rod connects the piston to the crank or crankshaft. The connecting rod has been the topic of research for different aspects such as manufacturing, materials, performance simulation, fatigue, etc. A four-stroke engine is the most common type. The four strokes are intake, compression, power, and exhaust. Each stroke requires approximately 180 degrees of crankshaft rotation, so the complete cycle would take 720 degrees. Each stroke plays a very important role in the combustion process. In the intake cycle, while the piston moves downward, one of the valves open. This creates a vacuum, and an air-fuel mixture is sucked into the chamber (Figure 1.1 (a)). During the second stroke compression occurs. In compression both valves are closed, and the piston moves upward and thus creates a pressure on the piston, see Figure 1.1 (b). The next stroke is power. During this process the compressed air-fuel mixture is ignited with a spark, causing a tremendous pressure as the fuel burns. The forces exerted by piston transmitted through the connecting rod moves the crankshaft, see Figure1.1(c). Finally, the exhaust stroke occurs. In this stroke, the exhaust valve opens, as the piston moves back upwards, it forces all the air out of the chamber and thus which completes the cycle of crankshaft rotation Figure 1.1(d)[2].

Automobile internal combustion engine connecting rod is a high volume production critical component. The CR is subjected to a complex state of stress. It undergoes high cyclic loads of the order of 10^8 to 10^9 cycles, which range from high compressive loads due to combustion, to high tensile loads due to inertia. In modern automotive internal combustion engines, the connecting rods are most usually made of steel for production engines, but can be made of carbon composite fiber , aluminum (for lightness and the ability to absorb high impact at the expense of durability) or titanium (for a combination of strength and lightness at the expense of affordability) for high performance engines, or of cast iron for applications such as motor scooters.

Fig 1.1(a) Intake Stroke

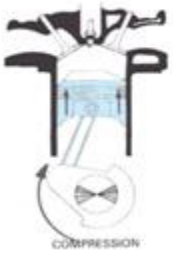

Fig 1.1(b) Compression Stroke

Fig 1.1(c) Power Stroke

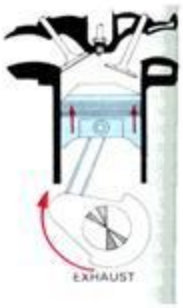

Fig 1.1(d) Exhaust Stroke

Figure 1: Different strokes of an Internal Combustion Engine

They are not rigidly fixed at either end, so that the angle between the connecting rod and the piston can change as the rod moves up and down and rotates around the crankshaft. Connecting rods, especially in racing engines, may be called "billet" rods, if they are machined out of a solid billet of metal, rather than being cast. The con rod is under tremendous stress from the reciprocating load represented by the piston, actually stretching and being compressed with every rotation, and the load increases to the third power with increasing engine speed. Failure of a connecting rod, usually called "throwing a rod" is one of the most common causes of catastrophic engine failure in cars, frequently putting the broken rod through the side of the crankcase and thereby rendering the engine irreparable; it can result from fatigue near a physical defect in the rod, lubrication failure in a bearing due to faulty maintenance, or from failure of the rod bolts from a defect, improper tightening, or re -use of already used (stressed) bolts where not recommended. This is because production auto parts have a much larger factor of safety, and often more systematic quality control.

1.2 Analytical Vector Approach

With reference to Figure 2, for the case of zero offset (e = 0), for any given crank angle θ, the orientation of the connecting rod is given by:

$\beta = \sin^{-1}\{-r_1 \sin\theta / r_2\}$

Angular velocity of the connecting rod is given by the expression:

$\boldsymbol{\omega 2} = \omega 2\ \mathbf{k}$

$\omega 2 = -\ \omega 1 \cos\theta / [(r_2/r_1)^2 - \sin^2\theta\ ]^{0.5}$

Note that bold letters represent vector quantities. The angular acceleration of the connecting rod is given by:

$\boldsymbol{\alpha 2} = \alpha 2\ \mathbf{k}$

$\alpha 2 = (1/\cos\beta\ )\ [\ \omega 1^2\ (r1/r2)\ \sin\theta - \omega 2^2\ \sin\beta\ ]$

Absolute acceleration of any point on the connecting rod is given by the following equation:

$\mathbf{a} = (-r1\ \omega 1^2\ \cos\theta - \omega 2^2\ u\ \cos\beta - \alpha 2\ u\ \sin\beta)\ \mathbf{i} + (-r1\ \omega 1^{\ 2}\ \sin\theta - \omega 2^2\ u\ \sin\beta + \alpha 2\ u\ \cos\beta)\ \mathbf{j}$

Acceleration of the piston is given by:

$\mathbf{ap} = (-\omega 1^2\ r1\ \cos\theta - \omega 2^2\ r2\ \cos\beta - \alpha 2\ r2\ \sin\beta)\ \mathbf{i} + (-\omega 1^2\ r1\ \sin\theta - \omega 2^2\ r2\ \sin\beta + \alpha 2\ r2\ os\beta)\mathbf{j}$

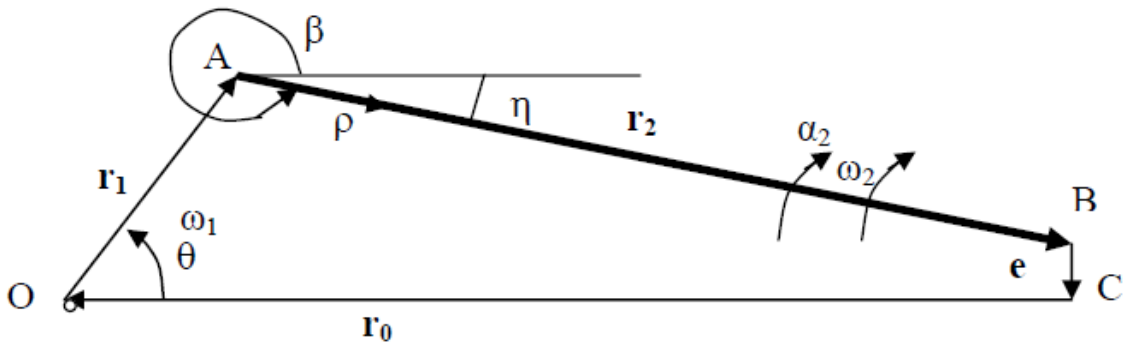

Figure 2 Vector representation of slider-crank mechanism.

Forces acting on the connecting rod and the piston are shown in Figure 4.6. Neglecting the effect of friction and of gravity, equations to obtain these forces are listed below.

Note that mp is the mass of the piston assembly and mc is the mass of the connecting rod. Forces at the piston pin and crank ends in X and Y directions are given by:

FBX = – (mp aP + Gas Load)

FAX = mc ac.gX - FBX

FBY = [mc ac.gY u cosβ - mc ac.gX u sinβ + Izz α2 + FBX r2 sinβ] / (r2 cosβ)

FAY = mc ac.gY - FBY

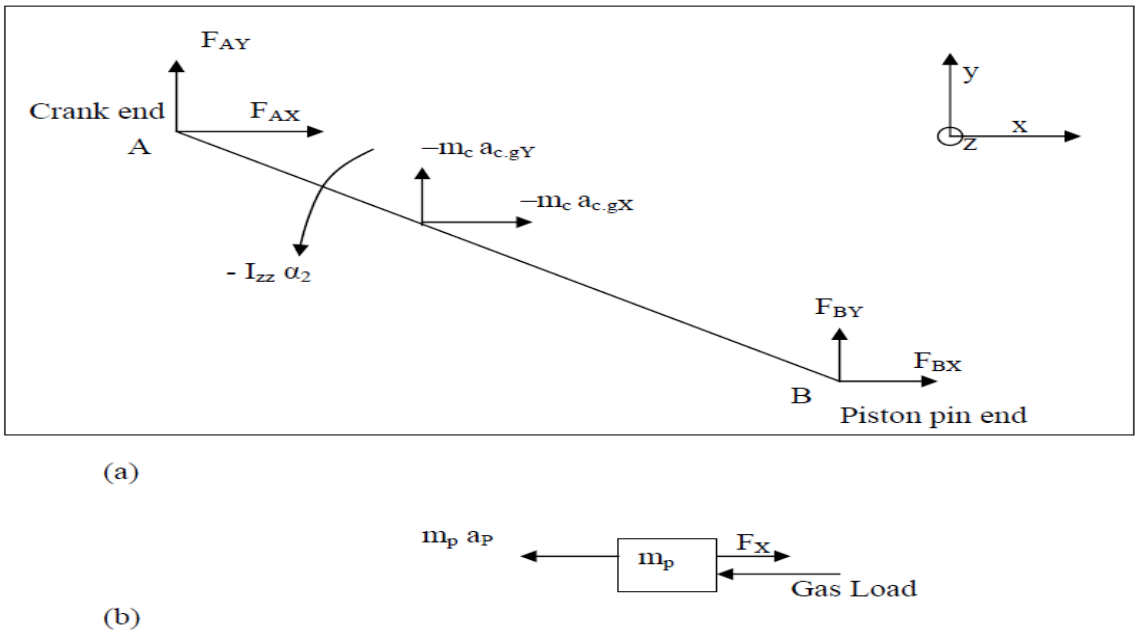

Figure 3. Free body diagram and vector representation. (a) Free body diagram of connecting rod. (b) Free body diagram of piston.

These equations have been used in an EXCEL spreadsheet. This program provides values of angular velocity and angular acceleration of the connecting rod, linear acceleration of the crank end center, and forces at the crank and piston pin ends. These results were used in the FE model while performing quasi-dynamic FEA. An advantage of this program is that with the availability of the input and the output could be generated in a matter of minutes. This is a small fraction of the time required when using commercial software's. When performing optimization, this is advantageous since the reactions or the loads at the connecting rod ends changed with the changing mass of the connecting rod.

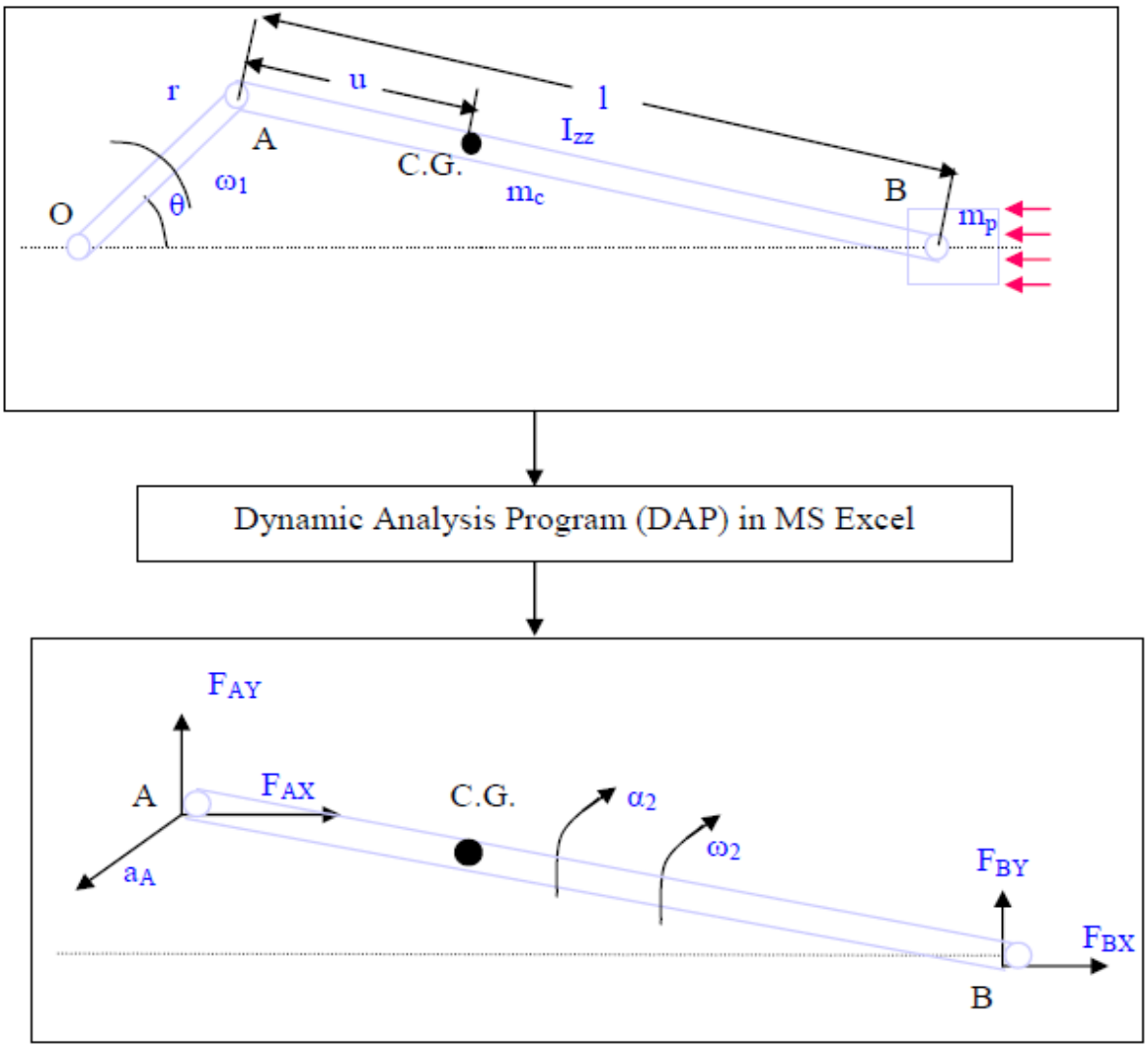

Figure 4: Typical input required for performing load analysis on the connecting rod and the expected output.

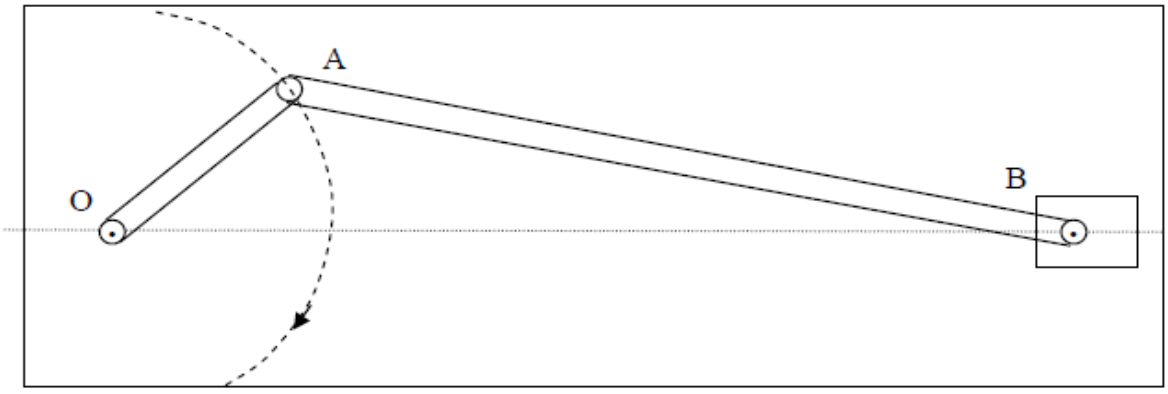

Figure 4: 'Slider-crank mechanism –1'.

To calculate stress in each connecting rod parts, calculated forces for each parts was exerted on corresponding parts. Inertia forces were evenly exerted on pin end inner level.

$$P_i = \frac{F_i}{2R_m l_s} \qquad (N/m^2)$$

Where,

$P\,i$ is force per unit area (N/m^2),

$l\,s$ is pin end width (m),

$F\,i$ is inertia force and

$R\,m$ is pin end mean radius (m).

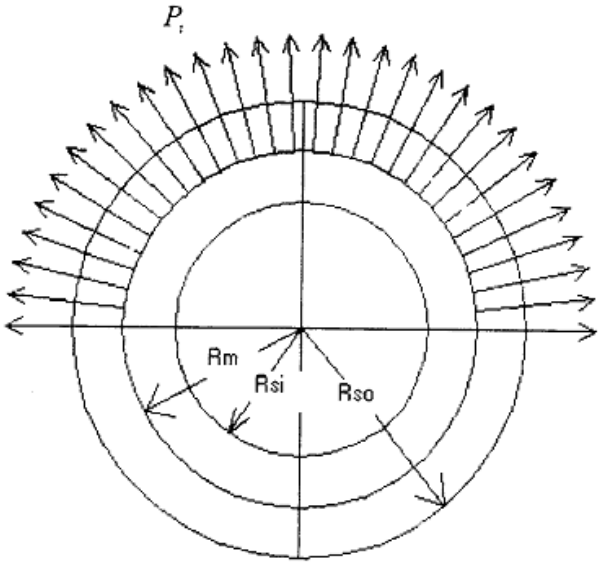

Fig. 5: Inertia force distribution on pin end.

2. The force resulted from combustion pressure were sinusoidal exerted on pin end inner level (figure 4.10). The value of this force was calculated using following formula:

$$P_g = \left(\frac{2F_g}{\pi\ R_m l_s}\right)\sin\theta \quad (N/m^2)$$

Where,

P_g is force per unit area (N/m2) and

F_g is force resulted from combustion (N)

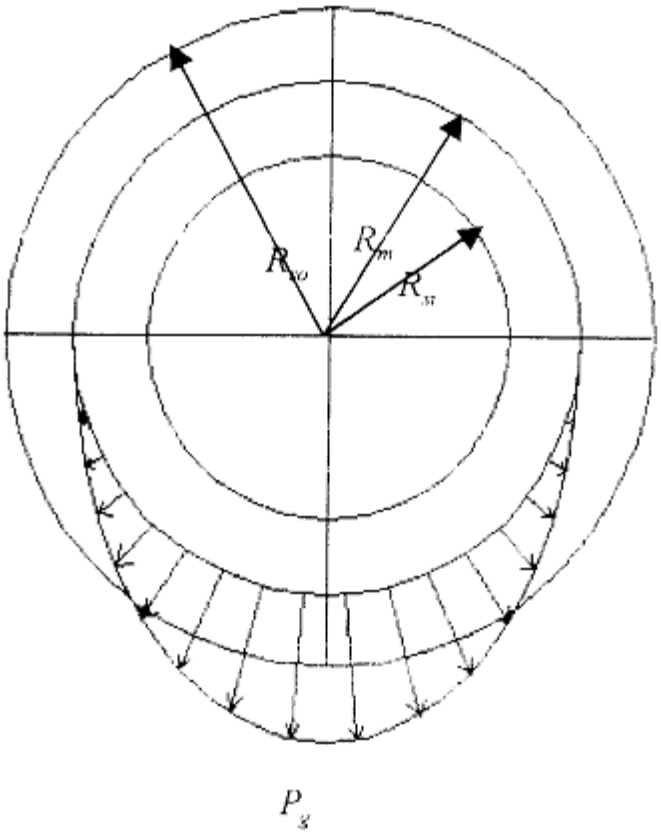

Fig 6: pressure force distribution on pin end.

The force resulted from falsifying of pin end's linier and also from friction between liner and piston pin were evenly exerted on pin end inner level all situations. These forces cause pressure stress in linier and tensile stress in connecting rod. This pressure was calculated using following formula:

$$P_b = \frac{\Delta_{tot}}{d_{su}\left[\frac{(d_{su}^{\ 2}+d_{si}^{\ 2})(d_{su}^{\ 2}-d_{si}^{\ 2})+U}{E_S}+\frac{(d_{su}^{\ 2}+d_{si}^{\ 2})/(d_{sa}^{\ 2}-d_{si}^{\ 2})-U}{E_b}\right]}$$

Where,

$\Delta\, tot$ is sum of initial diameter differences and diameter differences resulted from friction (m),

$d\, su$ is pin end's outer diameter (m),

$d\, si$ is pin end's inner diameter (m),

U is Poisson ratio and

E_s, E_b is elasticity module of connecting rod and linier (Pa).

2. Literature Review

2.1. Characterization and Mechanical Behavior of Composite Material Using FEA

S. Irfan Sadaq1, Dr. N. Seetharamaiah2, J. Dhanraj Pamar3, Afroz Mehar4 Department of Mechanical Engineering, Muffakham Jah College of Engineering & Technology, Hyd.

In above said paper composite laminates made of glass fiber and epoxy resin are tested to find the strength of the laminate and also its mechanical properties. By using FEA (Ansys the optimum helix angle is determined for the composite material. The paper fails to validate the results with any analytical method and any analysis of a laminate will involve modelling on FEM which will be a time consuming process. Further the results from FEA deviate a lot from those of the actual samples.

2.2. Research On Finite Element Analysis Of Composite Materials

Valeriu DULGHERU, Viorel BOSTAN, Marin GUȚU Technical University of Moldova gutumarin@ymail.com

This paper also verified the accuracy of composite materials data input into ANSYS Parametric Design Language for the numerical analysis. For this purpose, some specimens of the laminated composite were subjected to a bending moment and the deformations were measured. At the same time, the data obtained by simulating the specimens with the help of ANSYS APDL, were analyzed and compared to the experimental data in order to establish the degree of the accuracy.

2.3. *(Gopinath and Sushma, 2015). (Hui et al., 2015)* conducted experimental and simulation studies of buckling behavior of CR. It was pointed out that conventional analytical equations have limitations in applications as they are derived from ideal conditions for a strut in compression and should be addressed properly while attempting to reduce weight of CR. It was concluded that buckling stress measured in test rig falls closer to the FE simulation results due to collective use of first and second modes of buckling behaviour.

2.4. *(Webster et al., 1983)* performed three dimensional finite element analysis of a high-speed diesel engine connecting rod. For this analysis they used the maximum compressive load which was measured experimentally, and the maximum tensile load which is essentially the inertia load of the piston assembly mass. The load distributions on the piston pin end and crank end were determined experimentally.

2.5. In a study reported by *(Repgen, 1998),* based on fatigue tests carried out on identical components made by powder metallurgy and drop forging of fracture splitting steel. It was noticed that the fatigue strength of the forged steel component is 21% higher than that of the powder metal. These factors suggest that a fracture splitting material would be the material of choice for steel forged connecting rods.

2.6. *(Park et al., 2003) investigated* micro structural behavior at various forging conditions and recommend fast cooling for finer grain size and lower network ferrite content for a CR made of fracture splitting steel. It was concluded that laser notching exhibited best fracture splitting results, when compared with broached and wire cut notches.

2.7. *(Sarihan and Song, 1990),* conducted studies on optimization of the wrist pin end design of a CR with an interference fit. The maximum loads in the whole operating range of the engine were used to design the CR. To design for fatigue, modified Goodman equation with alternating octahedral shear stress and mean octahedral shear stress was used. For optimization, they generated an approximate design surface, and performed optimization of this design surface. The objective and constraint functions were updated to obtain precise values. This process was repeated till convergence was achieved. They also included constraints to avoid fretting fatigue. The mean and the alternating components of the stress were calculated using maximum and minimum values of octahedral shear stress. Their exercise reduced the connecting rod weight by nearly 27%.

In view of the above research papers, different aspects of static and dynamic analysis should be considered while designing a CR. Therefore, objective of the present study is to design the CR, on the basis of static and dynamic load analysis for a saloon car (with 1.4L Diesel Engine) and optimizing for its weight by the use of FRP.

3. Motivation & objective

In this work connecting rod is replaced by Fiber Reinforced Plastic material . And it also describes the modelling and analysis of connecting rod. Composites have been utilized to solve challenging technological problems since a very long time, but the true potential of composite structures and technology began to be exploited with the breakthroughs in automobile where every once counts and for each pound of weight cut, the world goes faster and greener by a mile.

The design consists of various stages, the pre-design stage is the most crucial stage as it involves material selection and preliminary composite laminate analysis to determine possible stacking sequence of a laminate taking in account different variables. This data can be then further modelled into complex geometries for final detailed analysis.

Since most of the existing design tools are less developed for composites than for conventional materials, experimental testing is still widely used to validate design and analysis models. Some FEM solutions do offer composite analysis capability but the analysis is not simple as with isotropic materials and usually involve high computational time and cost. It is also required that the models for analysis are perfectly tuned and validated against the experimental data.

4. Selection of Material

The connecting rod is under tremendous stress from the reciprocating load represented by the piston, actually stretching and being compressed with every rotation, and the load increases to the third power with increasing engine speed. Steel is normally used for construction of automobile connecting rods because of its strength, durability, and lower cost. However, steel with its high mass density exerts excessive stresses on the crankshaft of a high speed engine. This in turn requires a heavier crankshaft for carrying the loads and, therefore, the maximum RPM of the engine is limited. Additionally, higher inertia loads, such as those caused by steel connecting rods and heavier crankshafts reduces the acceleration or declaration rates of engine speed. The automobile engine connecting rod is a high volume production, critical component. It connects reciprocating piston to rotating crankshaft, transmitting the thrust of the piston to the crankshaft. Every vehicle that uses an internal combustion engine requires at least one connecting rod depending upon the number of cylinders in the engine. With steel forging, the material is inexpensive and the rough part manufacturing process is cost effective. Bringing the part to final dimensions under tight tolerance results in high expenditure for machining, as the blank usually contains more excess material. The first aspect was to investigate and compare fatigue strength of steel forged connecting rods with that of the powder forged connecting rods. Due to its large volume production, it is only logical that optimization of the connecting rod for its weight or volume will result in large-scale savings. It can also achieve the objective of reducing the weight of the engine component, thus reducing inertia loads, reducing engine weight and improving engine performance and fuel economy. A composite is a material that is formed by combining two or more materials to achieve some superior properties. Almost all the materials which we see around us are composites.

The term "composite" refers to any material constituting two or more substances with significantly different properties - physical and chemical, which remain integrated yet distinct in the final load bearing structure. Normally they are used in form of layers of woven fibers or flat tapes wetted in a resin system.

In terms of strength; careful design, appropriate material selection and cautious fabrication of composites can yield much stronger, stiffer and lighter structures than similarly loaded metallic parts.

However the design of a fiber-reinforced composite structure is considerably more difficult than that of a metal structure, principally due to the difference in its properties in different directions. Every composite structure consists of different layers called plies which can have different material properties and thickness. Therefore a composite structure can have several stacking sequence which can differ with the number of layers, material properties and orientation of each layer are used for analysis on CR.

5. Methodology

A Connecting Rod of a saloon car 1.4litre diesel engine was procured in as forged and normalized condition. A full scale model of the CR was created using solid modeling software with the help of the geometry details captured from a blue light 3D scanner as shown in the Fig. 8. To test the mechanical properties of the CR material, a rectangular piece was taken using wire-cut EDM (Electric discharge machining) and a small sub sized tensile specimen (shown in Fig. 9) was prepared and tested in uniaxial tension in a 50kN UTM (Table top).

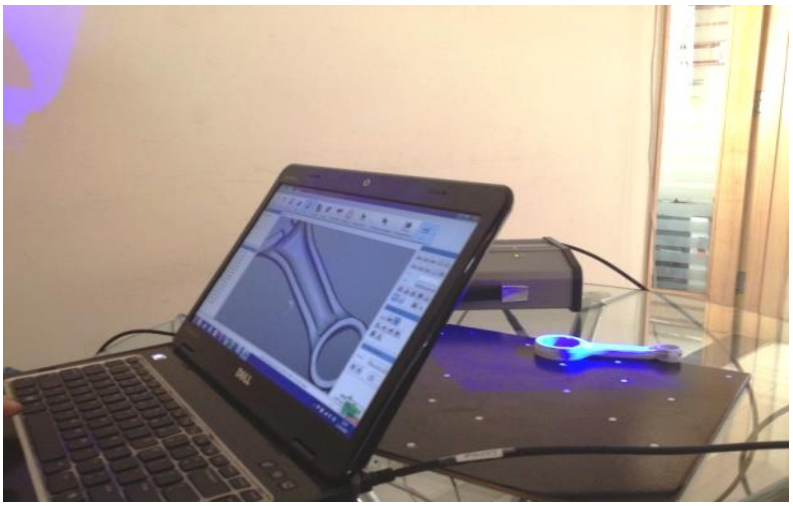

Fig.8 Blue light scanning of a CR using a scanner

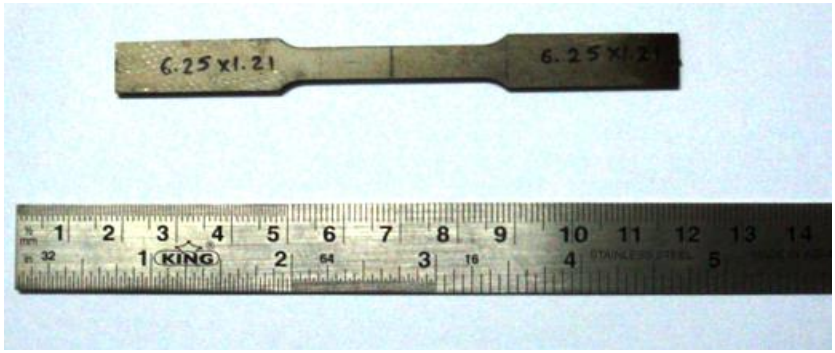

Fig.9 Sub sized tensile specimen of AISI4130

A pressure v/s Crank angle reading was collected using dedicated lab view software with the help of a computer attached to a CI Engine and various sensors. The specification of the diesel engine is given in Table 1. The calculations of the force, angular acceleration and angular velocity were calculated at various crank angles.

Table 1 Specifications of diesel engine used

Engine Type	In-line Engine
Engine Description	1.4 litre, 52.8bhp, 8V TDi Diesel Engine
Engine Displacement	1396
No. of Cylinders	4
Maximum Power	52.8bhp @5500rpm
Maximum Torque	85Nm@2500rpm
Valves per cylinder	2
Valves configuration	SOHC
Fuel supply system	MPFI
Bore X Stroke	75 X 79.5
Compression ratio	-
Turbo Charger	Yes
Super Charger	No

The details of the CR obtained by reverse engineering approach are observed as crank radius of 39.50mm with CR length of 125mm. The weight of the piston (measured with gudgen pin, piston rings and split lock ring) and CR are 557.29g and 578.53g respectively.

Pressure v/s crank angle curve was determined at various rpm 5000, 4000, 3000 and 1000 rpm with no load and maximum load conditions. The CR was designed for the worst condition i.e. maximum load and maximum rpm. The data for pressure variation with crank angle is captured from labview software and is shown in Fig. 10.

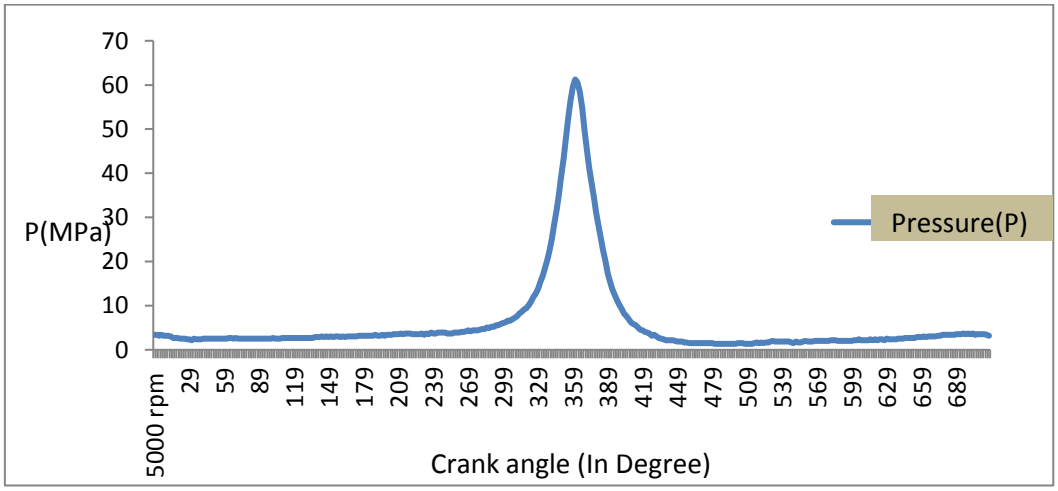

Fig. 10 Pressure V/s crank angle maximum load.

With these data, angular velocity and angular acceleration of the connecting rod, as well as linear accelerations of the connecting rod crank end center and of the center of gravity (CG)

can be obtained using theoretical approach (Athavale and Sajanpawar, 1991). The variation of angular velocity and angular acceleration are shown in Fig. 10 respectively. Similarly various components of forces in x-direction and y-direction at crank pin end and piston pin end are shown in Fig. 11 and Fig. 12 respectively. Stress at a point on the connecting rod as it undergoes a cycle consists of two components, a bending stress component and an axial stress component. The bending stress depends on the bending moment, which is a function of load at the CG normal to the connecting rod longitudinal axis, as well as angular and linear acceleration components normal to this axis. Therefore, for any given point on the connecting rod, the bending moment varies in an identical fashion between 0° and 360° crank angle as it varies between 360° and 720° crank angle. The axial load variation, however, does not follow the same cycle of repetitive pattern, as one cycle of axial load variation consists of the entire 720° crank angle. This is because of the variation in gas load, one cycle of which consists of 720° crank angle.

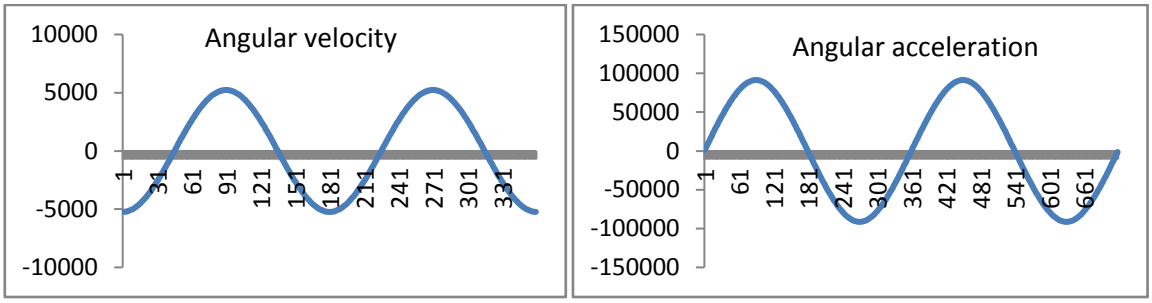

Fig. 11 Variations of angular velocity and acceleration of the connecting rod over one complete engine cycle at a crankshaft speed of 5000 rpm.

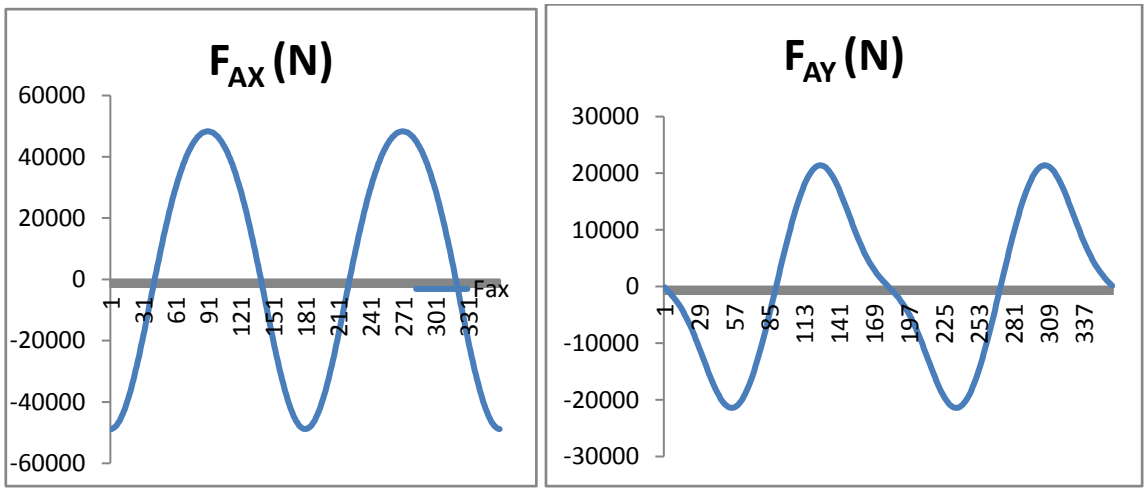

Fig. 12 Variations of the components of the force over one complete cycle at the crank end in x- direction and y-direction of the connecting rod at crankshaft speed of 5000 rev/min

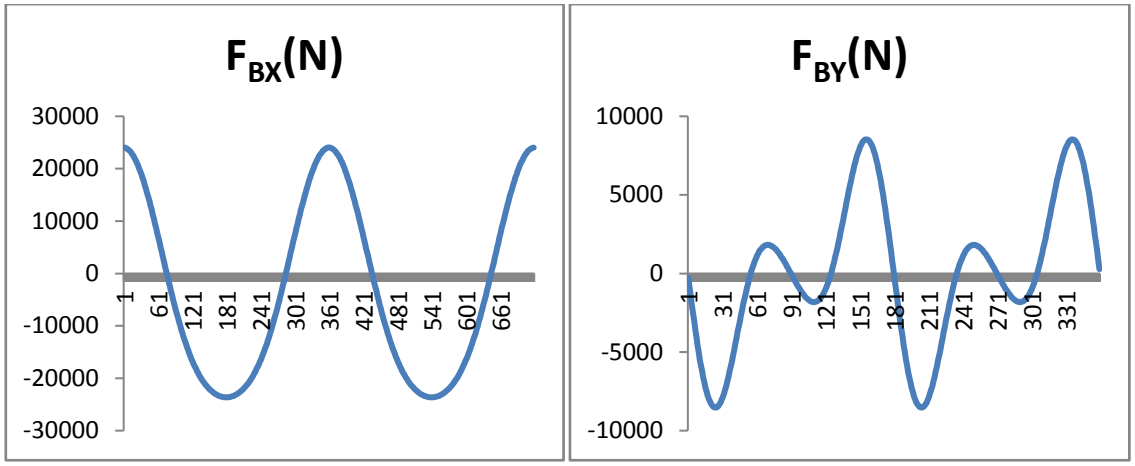

Fig. 13 Variations of the components of the force over one complete cycle at the Piston pin end in x- direction and y-direction of the connecting rod at crankshaft speed of 5000 rev/min

The laminates of FRP were then cut according to **ASTM standard** as seen in figure 13 below, for tensile tests using water abrasive jet cutting, utilising a cutting speed of 400 mm/min.

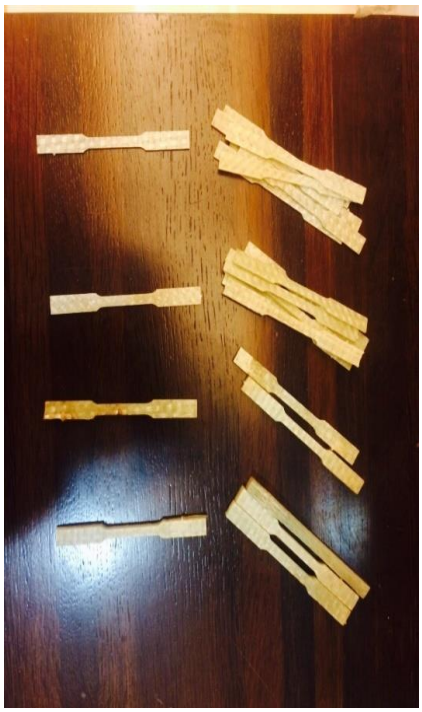

Figure 14. Bidirectional 2,3,4 & 8 Layer Laminate cut as per the standard subsize

The samples fabricated were of three different thickness and fiber orientation of 90 degrees and 45 degrees. These samples were then tested under tensile loading using the machine which provided us with load vs displacement curves for each of the test samples. The maximum load capacity of the machine was 50KN which limited the thickness of the samples

that could be tested and hence maximum thickness was limited to 2.0 mm. The loading speed employed was 5 mm/min. All the samples were cut according to the ASTM standards with width 5.02 mm and parallel length 40.04 mm.

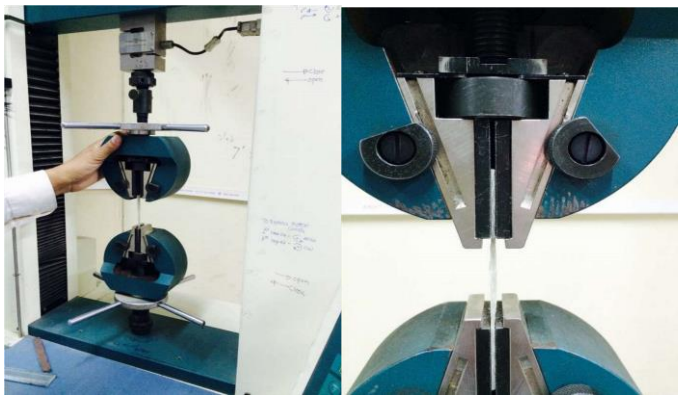

Figure 15 UTM Testing of the Composite Sample

All 16 samples were tested on the UTM under tensile tests. The next step was to apply force with successive increments on the samples and the corresponding deflection data was then recorded. Force vs. Deflection graph (Fig.11) is plotted for each sample and a comparison was drawn between the values of the experimental analysis, analytical analysis and FEA analysis (Fig.12).

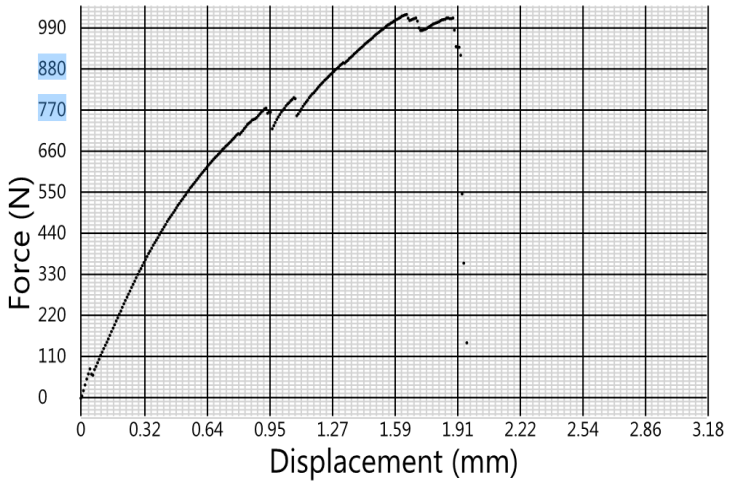

Fig 16: Force Vs. Deflection Graph of a 2 layer FRP Sample from UTM

6. Finite Element Analysis

Finite Element Analysis (FEA) is a numerical computation method that is used to analyze complex structures. FEA takes large bodies and breaks them into smaller finite elements. This is done because these finite elements are governed by mechanics equations that are simpler to solve than the one needed to analyze the entire structure. A computer can run many more simplified equations quickly, which makes these finite elements models ideal for analysis. These finite elements are given the material and geometric properties that would exist on the actual structure. Loads and constraints are applied to the model to simulate the operating environment. Then, the finite element solver calculates the strains, stresses, deflections, and other desired output of the structure under the load case. The FEA software used in this model is ABAQUS. It is important to run a study to determine the size of the mesh. The number of elements in a FEM is related to the precision attained. It is important to use just enough elements to have a precise model. With too many elements, the computation time is greatly increased and efficiency is lost. The tensile analysis of the Composite Laminate was carried out in ABAQUS 6.14.1 using the following procedure :-

- The model was made using AUTOCAD in .dxf format
- A planar shell of the subsize dimension was created

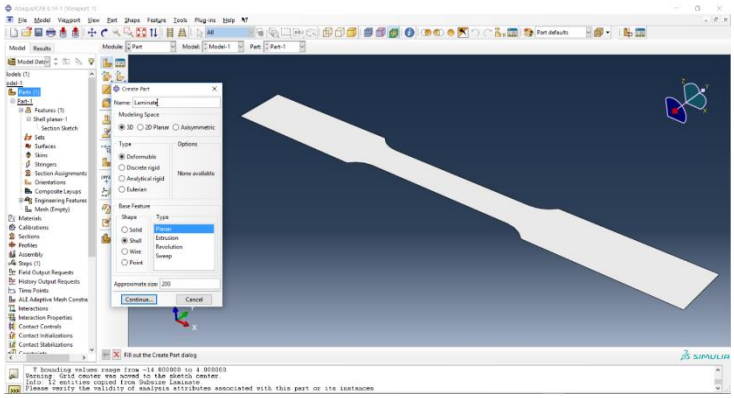

Figure 17. Modelling of Subsize laminate in ABAQUS 6.14.1

- The parts were appropriately partitioned for Mesh refinement and application of boundary conditions.
- The material properties were then added in the properties module, the material was given the properties of a Lamina and the fail stresses for each were given to separately calculate the failure of the different layers in the lamina.

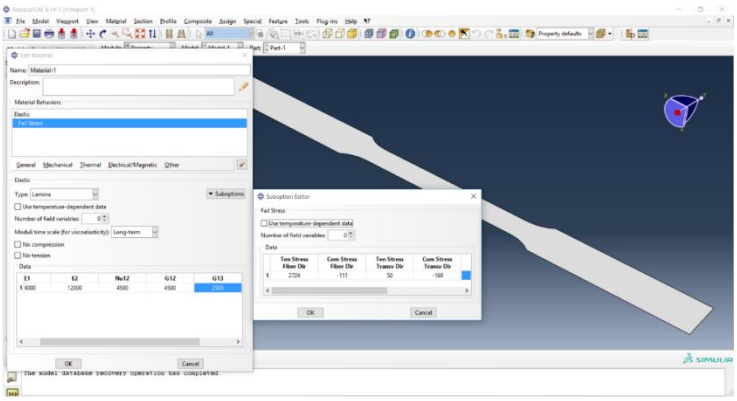

Figure 18 Addition of Material Properties

- Initially 2 layer laminate were modeled using the layup feature in the composite tab.

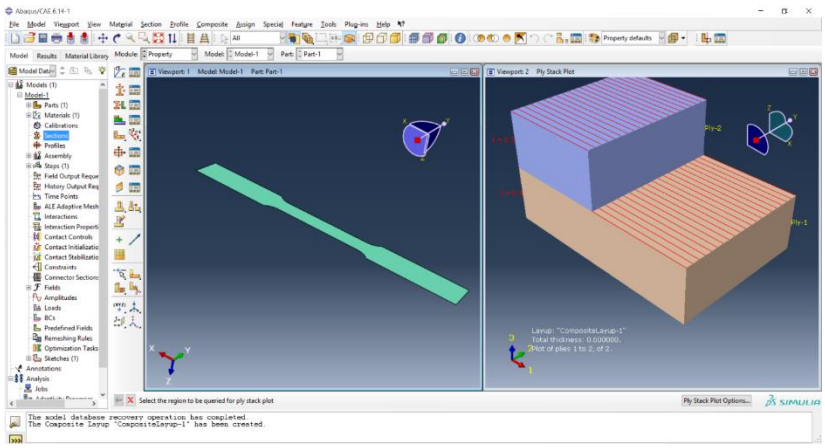

Figure 19 Layer stackup of 2 layer bidirectional GF Laminate

- Further for a uniform mesh global and local seeds were created and then the assembly was made

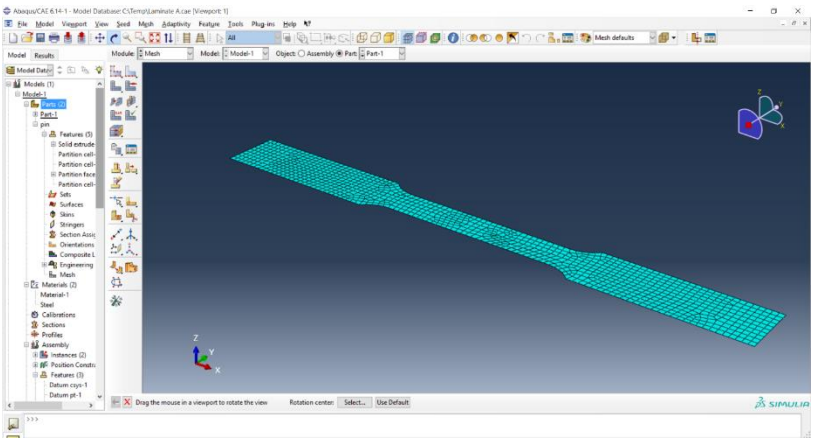

Figure 20 Mesh assembly for 3 Tensile Test

- Now the boundry conditions are applied on various points, edges and partitions of the assembly
- The maximum loads as per the experimental values were applied.

6.1.1Material properties of the layers:

Linear elastic properties used for the material:

E_{11} = 1.64e5 MPa,

$E_{22} = E_{33}$ = 1.2e4 MPa,

$G_{12} = G_{13}$ = 4500 MPa,

G_{23} = 2500 MPa,

$v_{12} = v_{13}$ = 0.32, and v_{23} = 0.45

The strength properties are:

Tensile failure stress in fiber direction: X_{1t} = 2724 MPa,

Compressive failure stress in fiber direction: X_{1c} = 111 MPa,

Tensile failure stress in direction 2: X_{2t} = 50 MPa,

Compressive failure stress in direction 2: X_{2c} = 1690 MPa,

Tensile failure stress in direction 3: X_{3t} = 290 MPa,

Compressive failure stress in direction 3: X_{3c} = 290 MPa,

Shear strength in 12 plane: S_{12} = 120 MPa,

Shear strength in 13 plane: S_{13} = 137 MPa,

Shear strength in 23 plane: S_{23} = 90 MPa

The strength properties are:

Tensile failure stress in fiber direction: X_{1t} = 1050 MPa,

Compressive failure stress in fiber direction: X_{1c} = 56 MPa,

Tensile failure stress in direction 2: X_{2t} = 40 MPa,

Compressive failure stress in direction 2: X_{2c} = 1100 MPa,

Tensile failure stress in direction 3: X_{3t} = 145 MPa,

Compressive failure stress in direction 3: X_{3c} = 145 MPa,

Shear strength in 12 plane: S_{12} = 90 MPa,

Shear strength in 13 plane: S_{13} = 110 MPa,

Shear strength in 23 plane: S_{23} = 60 MPa

Where the 1-direction is along the fibers, the 2-direction is transverse to the fibers in the surface of the ply, and the 3-direction is normal to the ply.

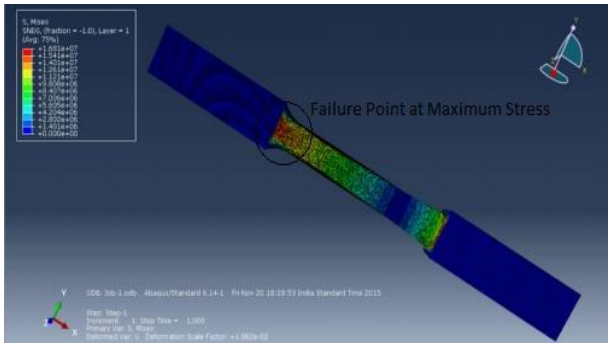

Fig 21: FEA Analysis- Simulation Results

6.2. FE Modelling and Simulation of the CR

For FE simulations, the flash along the entire connecting rod length including the one at the oil hole was eliminated in order to reduce the model size. The flash runs along the length of the connecting rod and hence does not cause stress concentration under axial loading. The flash is a maximum of about 0.15 mm thick. This initial simulation relied on a simple auto mesh. It may be necessary to mesh manually in subsequent simulations where the model is more detailed and the geometry is more complex. However, an auto mesh gives a reasonable estimate of stresses and the areas on which to concentrate for more detailed analyses. A solid model of the CR and a meshed model with 3D tetrahedron elements is shown in Fig.20.

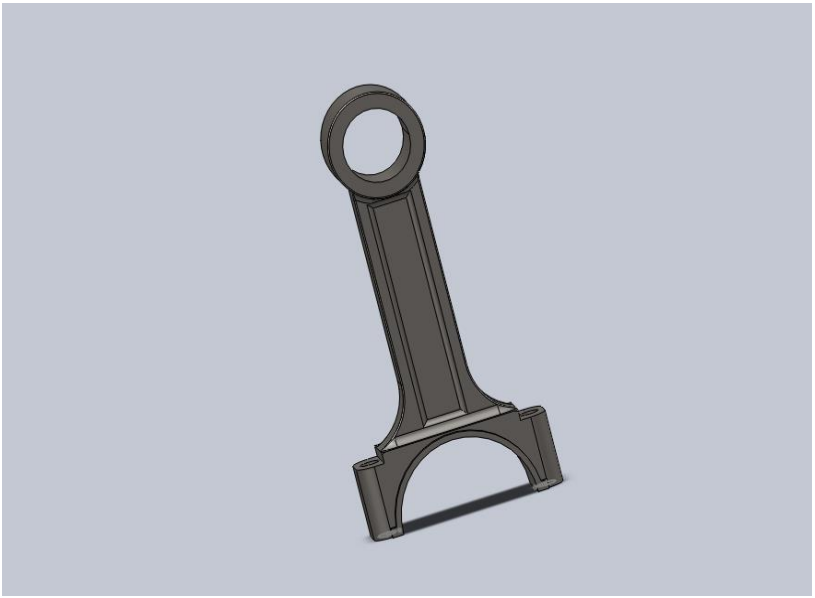

Fig 22 The top part1 of the connecting rod

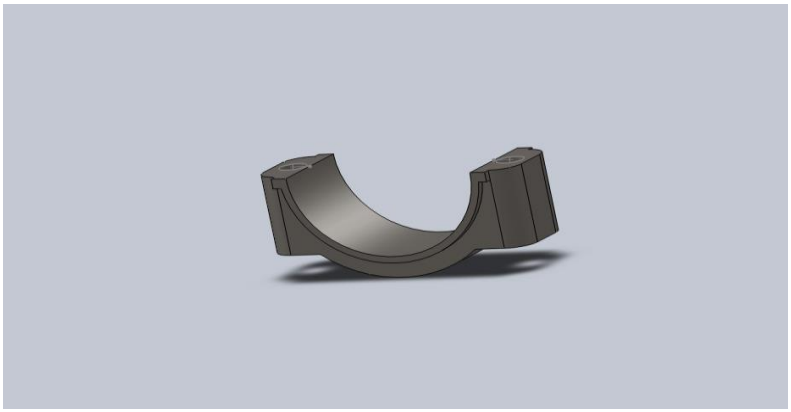

Fig 23 The bottom part2 of the connecting rod

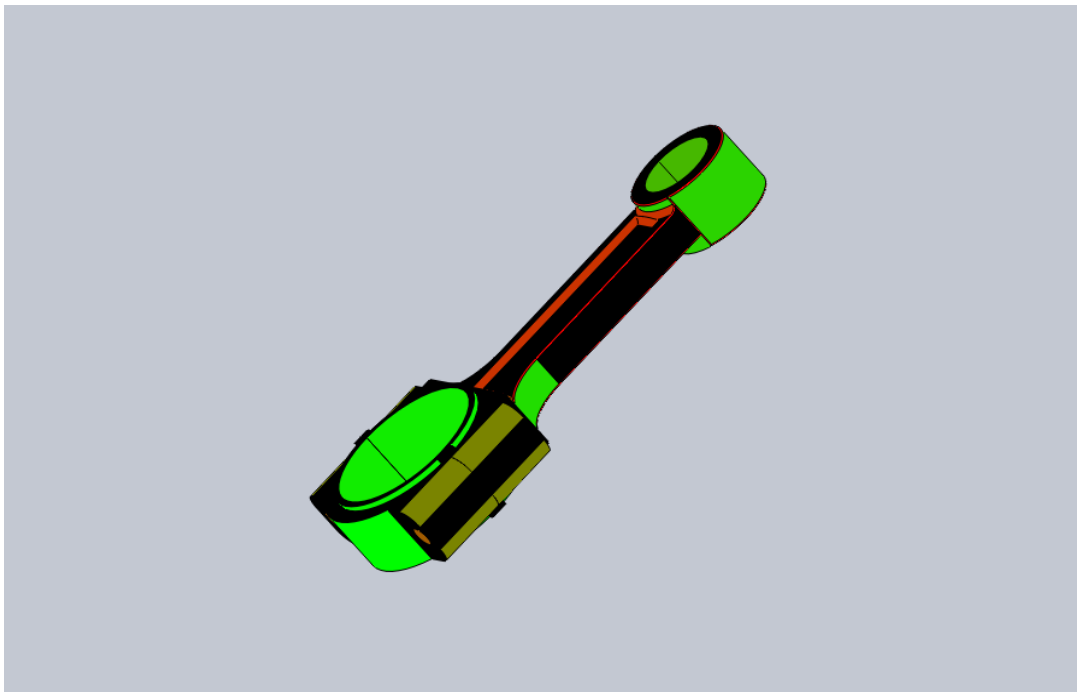

Figure 24: Geometry of the connecting rod assembly

6.3 Mesh Generation

6.3.1 Static FEA

This initial simulation relied on a simple auto mesh. It may be necessary to mesh manually in subsequent simulations where the model is more detailed and the geometry is more complex [12]. For this first analysis, however, an auto mesh gives a reasonable estimate of stresses and the areas on which to concentrate for more detailed analyses.

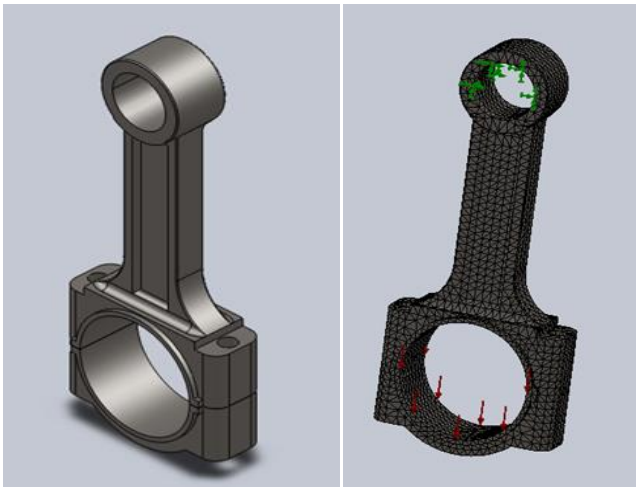

Fig. 25 Solid CAD model and 3D meshed model of CR

Table 2. Mesh quality details

Mesh type	Solid Mesh
Mesher Used	Standard mesh
Automatic Transition	Off
Include Mesh Auto Loops	Off
Jacobian points	4 points
Element size	3.17798 mm
Tolerance	0.158899 mm
Mesh quality	High
Total nodes	29526
Total elements	17632
Maximum Aspect Ratio	692.75
Percentage of elements with Aspect Ratio < 3	93.8
Percentage of elements with Aspect Ratio > 10	0.0284
% of distorted elements (Jacobian)	0

6.3.2 Quasi-Dynamic FEA

The same mesh that was used for static FEA, as presented in the section above, was also used for quasi-dynamic FEA. Convergence was checked at locations where high bending stresses are expected. In this case they were checked at locations.

6.4. Boundary Conditions and Loads

The forces on the connecting rod were calculated from the pressure distribution chart in the cylinder. The maximum pressure at the TDC will result in the maximum force onto the piston which will get transferred to connecting rod (neglecting friction force between piston rings and cylinder). Also, we are not considering the inertial forces due to acceleration change with

respect to crank angle, which may further add to pressure forces. The pressure variation chart is shown in Fig. 24. This acceleration was calculated by using kinematics theory. This method was used to generate data for various crank angles in Microsoft Excel. Angular acceleration values will be used in subsequent analyses to calculate the inertial loads. It seems that the connecting rod will always be in compression or bending but it is the inertial loads which will play the most important role in providing tensile loads at TDC just before the suction stroke. The maximum pressure in the cylinder at TDC is 61.24 MPa and area of the piston is 4417.86 mm^2. The product of both gives the force being experienced by the connecting rod.

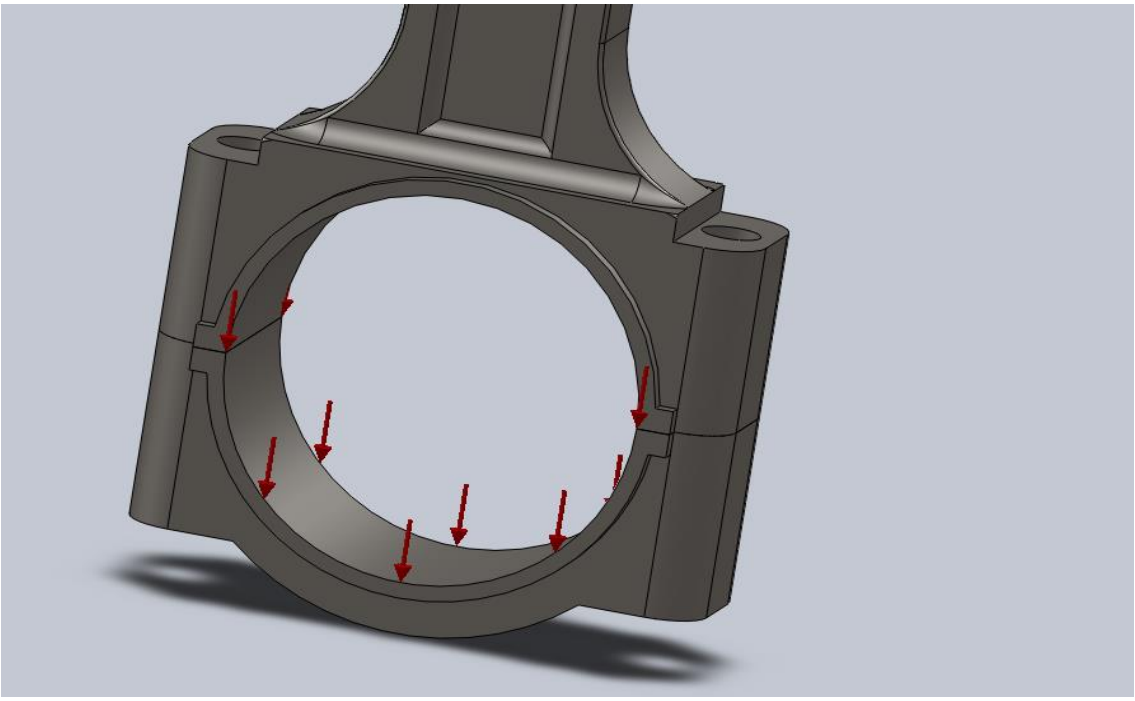

Figure 26: Tensile loading of the connecting rod

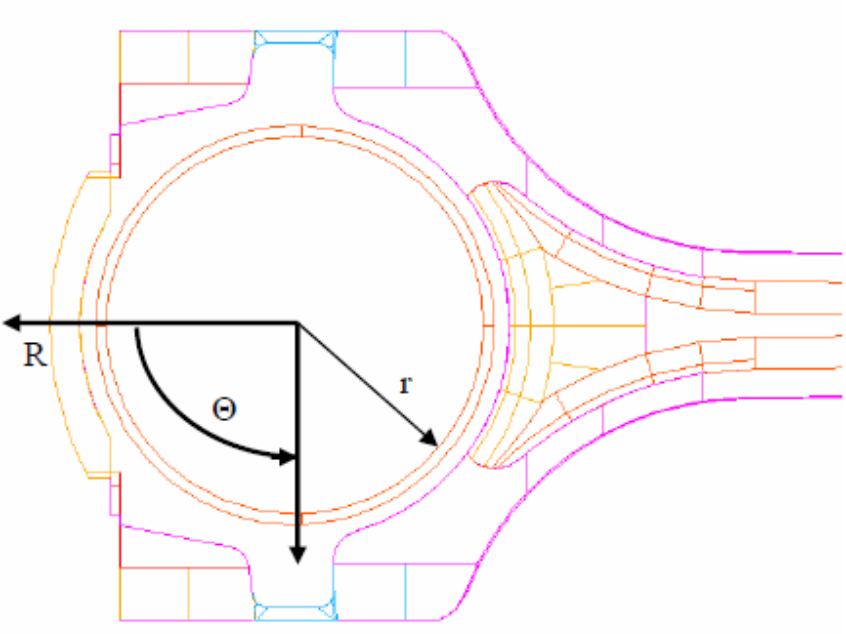

Figure 27: Polar co-ordinate system R, Θ, Z used. ‘t’ (not shown) is the thickness of the contact surface normal to the plane of paper.

7. Results and discussion

The uniaxial tension test of the tensile specimen of AISI4130 and FRP depicted the tensile strength as 810MPa and yield strength as 460MPa. The percentage elongation of the materials is found to be 24% as shown in Fig. 26. The other properties of the steel as given in Table 3 was taken from the literatures and used in FE simulations.

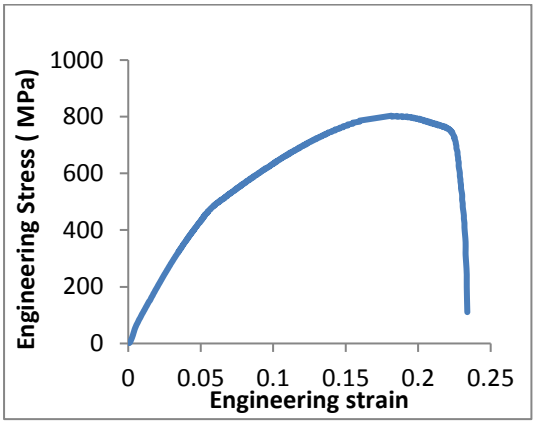

Elastic Modulus	205MPa
Poisson's ratio	0.285
Shear Modulus	80GPa
Density	7850 kg/m^3
Tensile Strength	731MPa
Compressive Strength	1070MPa
Yield Strength	460MPa
Thermal Conductivity	42.7 W/(m·K)
Specific Heat	477 J/(kg·K)

Fig. 28 Engineering stress strain plot for AISI4130 and other properties in Table 3.

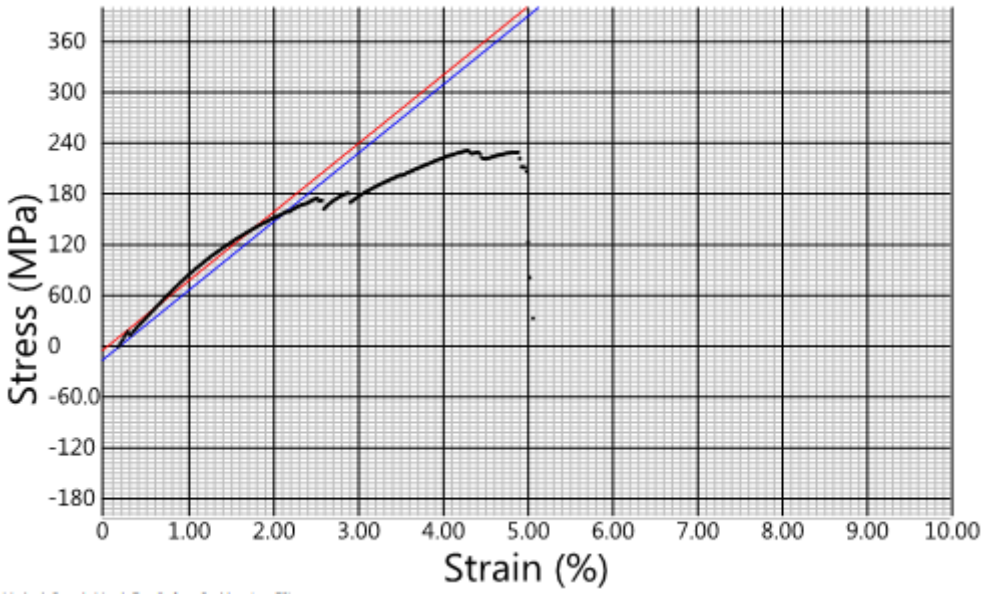

Fig. 29 stress v/s strain plot for FRP

Stress analysis is done at the worst loading criteria, giving the maximum forces on the connecting rod. The stress analysis is done in two different ways. In the first, the piston end was restrained and load/pressure is applied at the crank end, giving tensile forces on the connecting rod. In the Second case, the crank end is restrained and the load is applied at the piston end giving compressive forces on the connecting rod. It is observed

from stress analysis that in the first case when the compressive load is applied at the big end of the CR, the maximum stress is 183MPa and is shown in Fig 26. Whereas in the second case when the compressive load is applied at the small end of the CR, the maximum stress observed is 287MPa. The location of this high stress value is at the junction of the central portion and small end of the CR as shown in Fig. 28. The factor of safety of design is approximately 1.6 for worst load condition i.e. bucking. Tensile bending stresses were about 24% of the stress amplitude (entire operating range) at the start of crank end transition and about 27% of the stress amplitude (entire operating range) at the shank centre. Bending stresses were negligible at the piston pin end. It is understood that high strength materials will make the CR lighter and smaller in dimensions as the factor of safety of design will enhance further thereby necessitating the lowering of the dimensions of the CR.

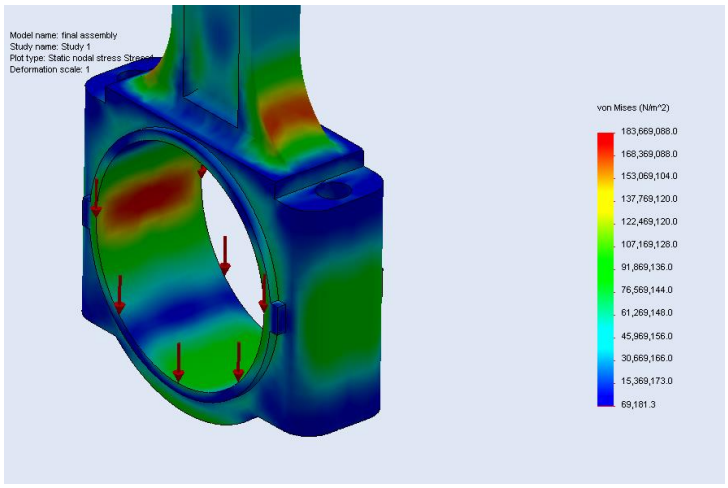

Fig. 30 Von Mises stress pattern in the big end of CR

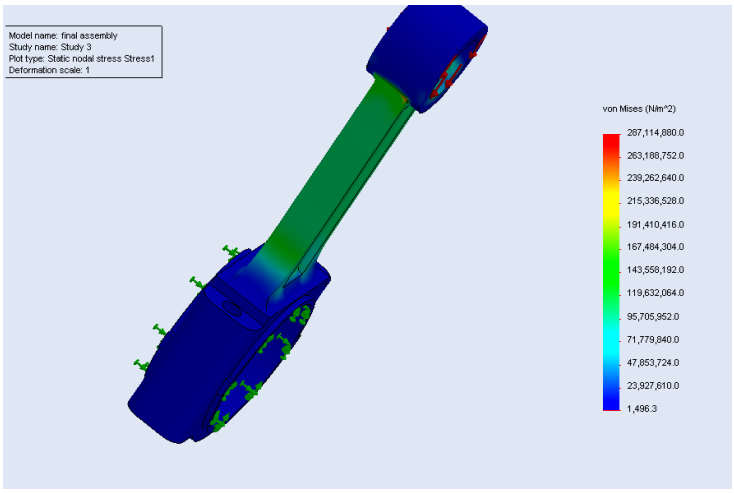

Fig. 31 Von Mises stress pattern in the small end of CR

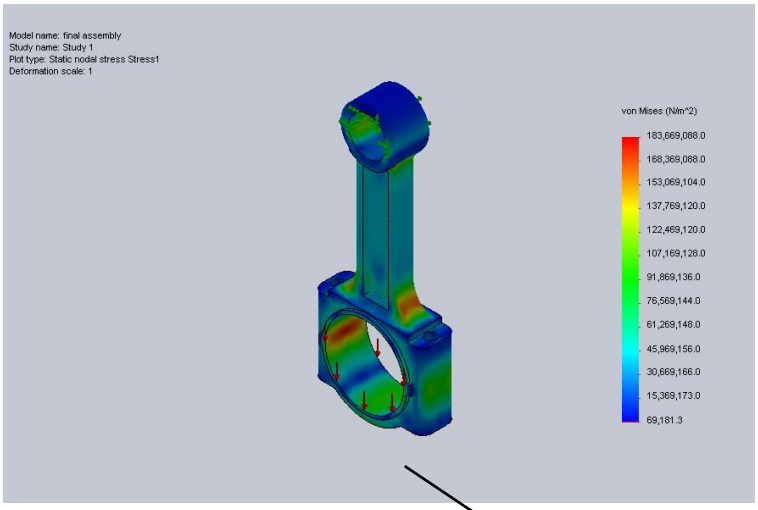

Fig 32: Von mises Stress shown on connecting rod-Isometric view

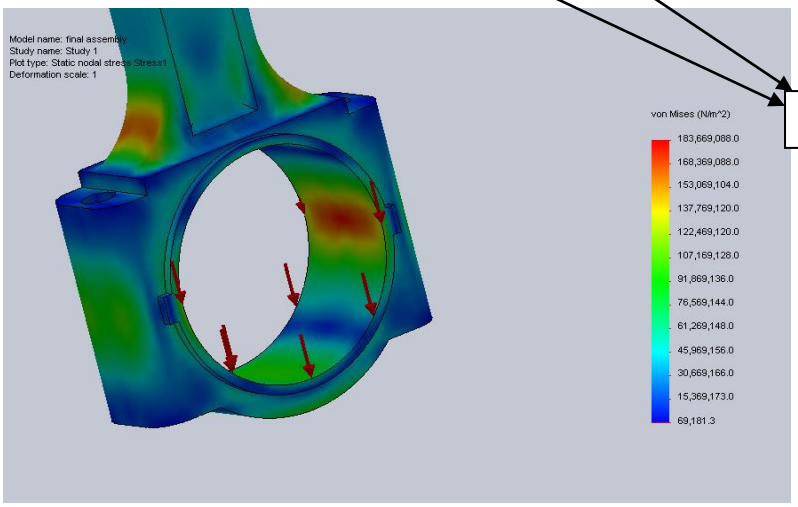

Fig 33 Von mises Stress shown at the corners

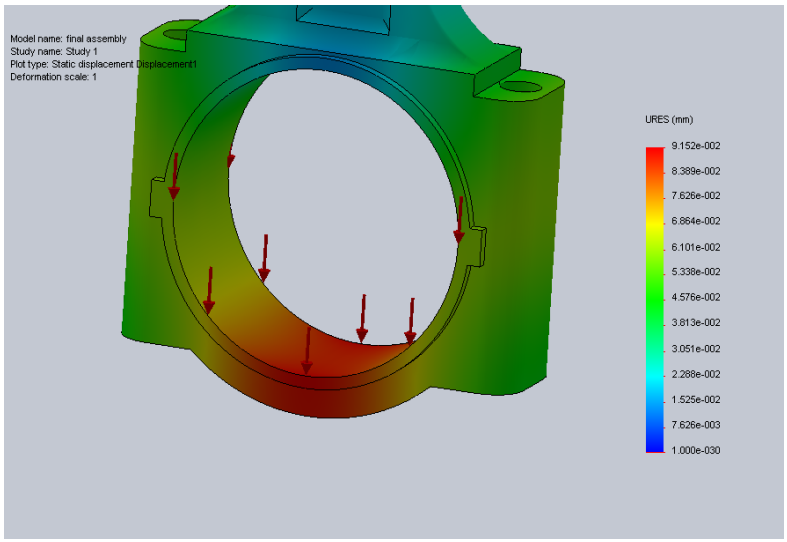

Fig 34 Displacement shown at crank end

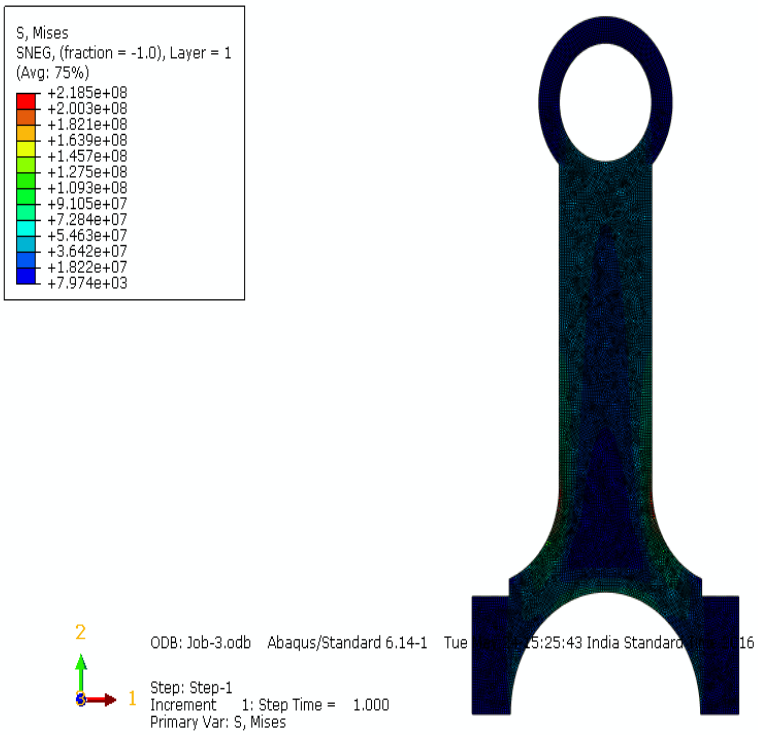

Figure 35 Layups all 90 degrees in Compression

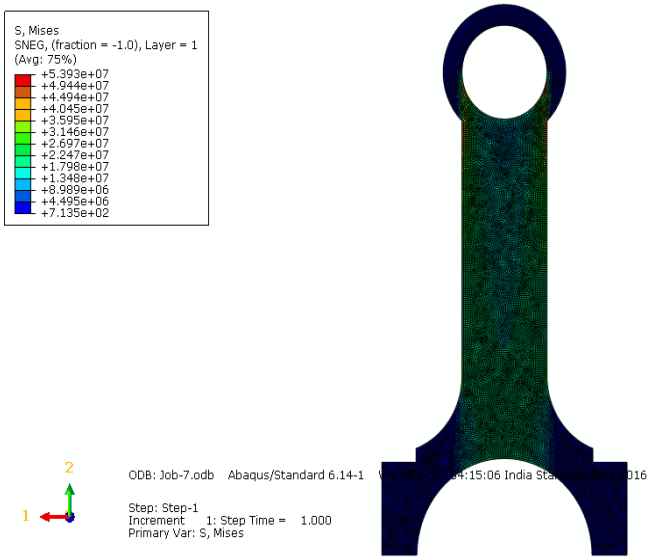

Figure 36 Layups all in 90 degrees in Tension

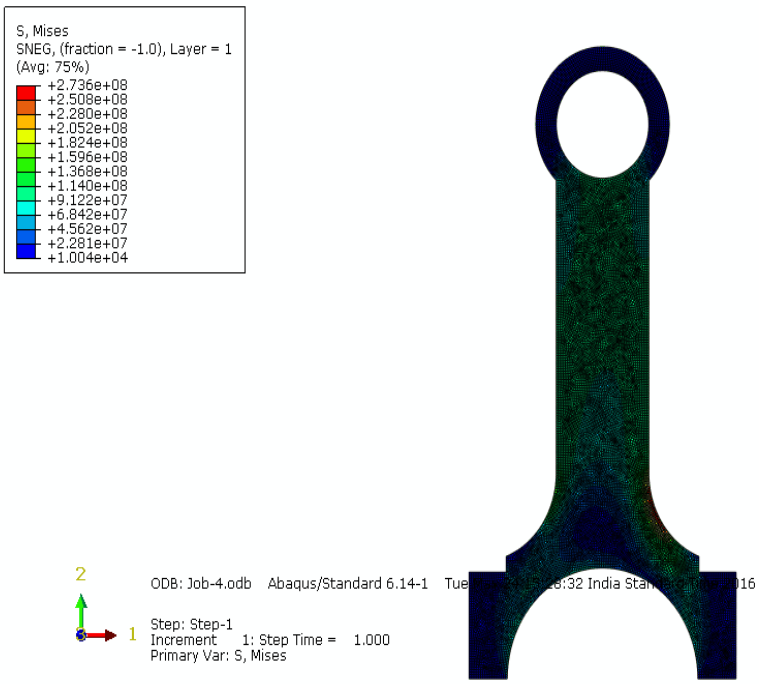

Figure. 37 Layups in 0,45,90 degrees in compression

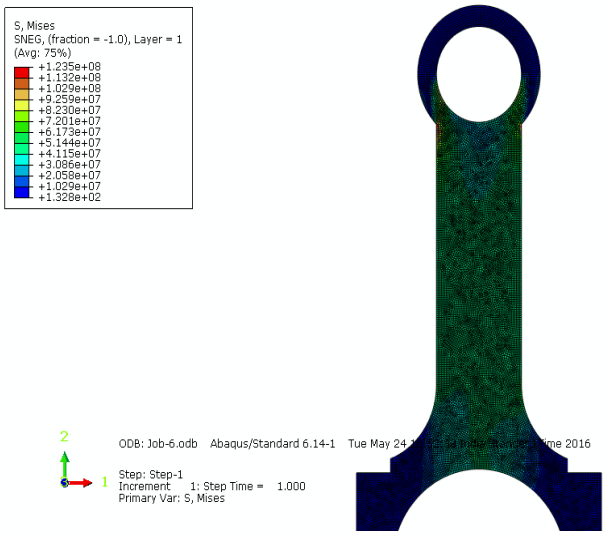

Figure. 38 Layups in 0,45,90 degrees in Tension

Tab 4: Comparison of mechanical Properties

Parameter's/Material	Steel (AISI4130)	FRP
Displacement (mm)	0.0137	0.2801e-03
Stress (N/mm2)	460.21	75.5887
Strain	0.04786	0.464E-04
Ultimate tensile strength	810Mpa	230.58 MPa

8. Conclusions

This research project investigated weight and cost reduction opportunities that steel forged connecting rods offer. Load analysis was performed based on the input from the crank angle diagram obtained from the same diesel engine in I.C Engine lab , which comprised of the crank radius, piston diameter, the piston assembly mass, and the pressure-crank angle diagram, using analytical techniques and computer-based mechanism simulation tools. Dynamic load analysis was then performed using the results from the outputs from the Engine soft software. The maximum stress is observed at the junction of the central portion and small end of the CR and its magnitude is of order of 287MPa. The factor of safety of design in bucking is only 1.5. Bending stresses were significant and should be accounted for. Tensile bending stresses were about 24% of the stress amplitude (entire operating range) at the start of crank end transition and about 27% of the stress amplitude (entire operating range) at the shank centre. Bending stresses were negligible at the piston pin end. High strength materials will make the CR lighter and smaller in dimensions as the factor of safety of design will enhance further thereby necessitating the lowering of the dimensions of the CR. In this thesis, a broken connecting rod made of forged steel is replaced with and Fiber Reinforced Plastic. The materials are changed so that the weight of the connecting rod is less when carbon fiber is used than Forged Steel. The connecting rod is modeled and, forces are calculated. Analysis is done on the connecting rod using material steel and carbon fiber 280 GSM bidirectional. By observing the analysis results of steel 460 MPa and carbon fiber as 72.5887MPa which are very much less than their respect yield strength values

9. Appendix

9.1 Paper Presentation

A research paper on Modeling and simulations of a connecting rod of high strength steel for a CI engine already presented in MANFEX 2016 at Amity University.

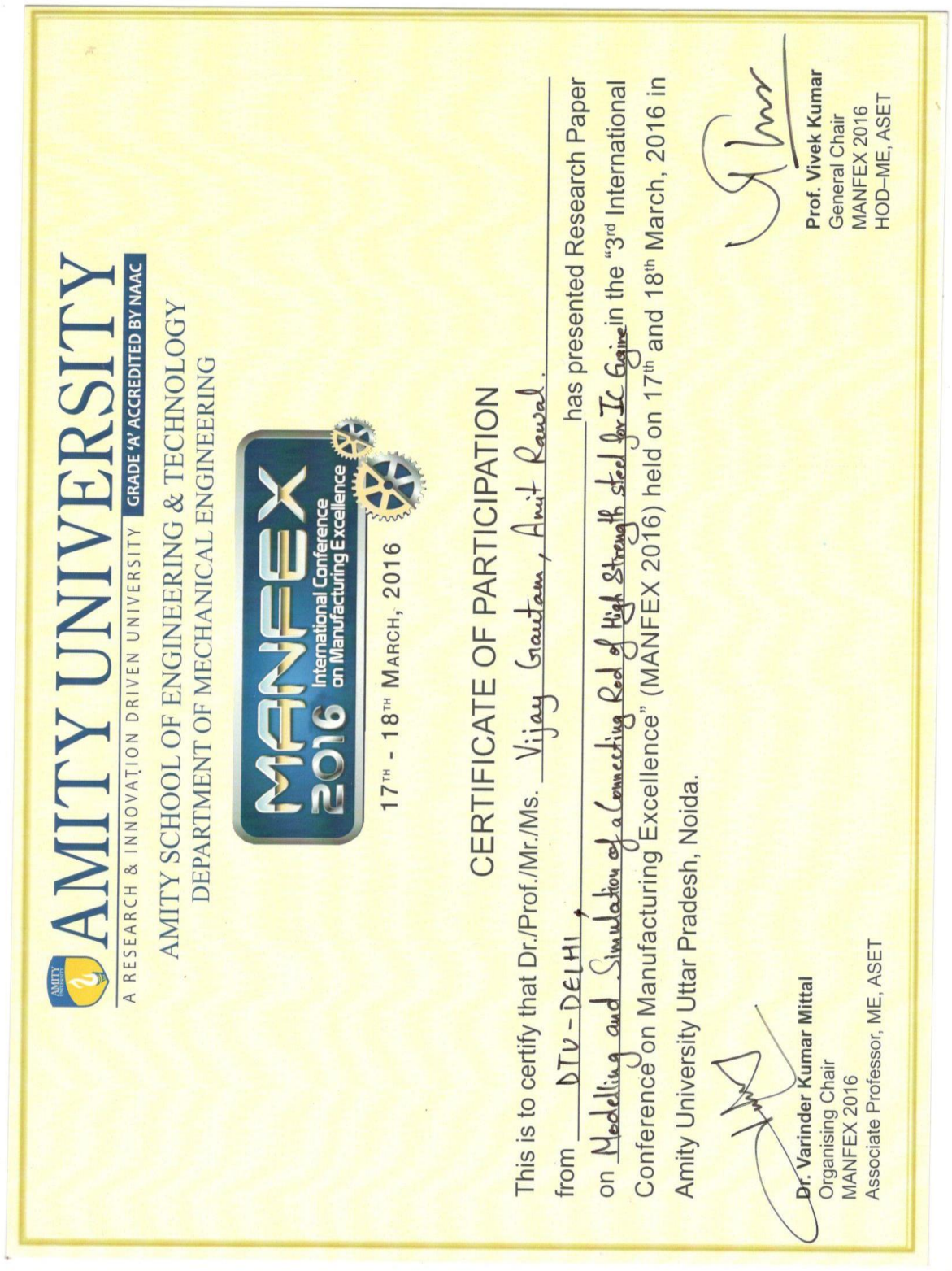

AMITY UNIVERSITY

A RESEARCH & INNOVATION DRIVEN UNIVERSITY GRADE 'A' ACCREDITED BY NAAC

AMITY SCHOOL OF ENGINEERING & TECHNOLOGY

DEPARTMENT OF MECHANICAL ENGINEERING

MANFEX 2016 International Conference on Manufacturing Excellence

17TH - 18TH MARCH, 2016

CERTIFICATE OF PARTICIPATION

This is to certify that Dr./Prof./Mr./Ms. Vijay Gautam, Amit Rawal

from DTU-DELHI,

has presented Research Paper on Modelling and Simulation of a Connecting Rod of High Strength steel for IC Engine in the "3rd International Conference on Manufacturing Excellence" (MANFEX 2016) held on 17th and 18th March, 2016 in Amity University Uttar Pradesh, Noida.

Dr. Varinder Kumar Mittal
Organising Chair
MANFEX 2016
Associate Professor, ME, ASET

Prof. Vivek Kumar
General Chair
MANFEX 2016
HOD–ME, ASET

9.2 Variation of Pressure against Crank Angles

SPEED	LOAD	ANGLE	CYL_PRESSURE	VOLUME	DIESEL_PRESSURE
rpm	kg	deg	bar	cc	bar
4964	-0.43	1	3.37	16.76	56.51
4964	-0.43	3	3.37	17.04	56.68
4964	-0.43	5	3.21	17.6	56.18
4964	-0.43	7	3.37	18.44	56.18
4964	-0.43	9	3.21	19.56	56.18
4964	-0.43	11	3.21	20.96	56.35
4964	-0.43	13	3.21	22.62	56.35
4964	-0.43	15	3.04	24.56	56.35
4964	-0.43	17	2.7	26.75	56.35
4964	-0.43	19	2.7	29.22	56.18
4964	-0.43	21	2.7	31.93	56.18
4964	-0.43	23	2.53	34.9	56.51
4964	-0.43	25	2.53	38.11	56.85
4964	-0.43	27	2.53	41.56	56.68
4964	-0.43	29	2.36	45.24	56.51
4964	-0.43	31	2.36	49.15	56.68
4964	-0.43	33	2.19	53.27	56.68
4964	-0.43	35	2.53	57.6	57.02
4964	-0.43	37	2.36	62.13	57.19
4964	-0.43	39	2.36	66.86	56.85
4964	-0.43	41	2.36	71.76	56.51
4964	-0.43	43	2.53	76.84	56.18
4964	-0.43	45	2.53	82.08	56.01
4964	-0.43	47	2.53	87.47	55.33
4964	-0.43	49	2.53	93.01	55.17
4964	-0.43	51	2.53	98.68	55

4964	-0.43	53	2.53	104.47	54.49
4964	-0.43	55	2.53	110.37	54.66
4964	-0.43	57	2.53	116.38	54.83
4964	-0.43	59	2.53	122.47	55
4964	-0.43	61	2.53	128.64	55.17
4964	-0.43	63	2.53	134.88	55.17
4964	-0.43	65	2.7	141.18	54.66
4964	-0.43	67	2.7	147.52	54.15
4964	-0.43	69	2.53	153.9	53.98
4964	-0.43	71	2.7	160.31	53.98
4964	-0.43	73	2.53	166.73	54.32
4964	-0.43	75	2.53	173.16	55
4964	-0.43	77	2.53	179.58	55.67
4964	-0.43	79	2.53	185.99	56.18
4964	-0.43	81	2.53	192.37	56.18
4964	-0.43	83	2.53	198.72	56.51
4964	-0.43	85	2.53	205.03	57.19
4964	-0.43	87	2.53	211.28	57.86
4964	-0.43	89	2.53	217.48	58.54
4964	-0.43	91	2.53	223.61	59.05
4964	-0.43	93	2.53	229.67	58.88
4964	-0.43	95	2.53	235.64	58.37
4964	-0.43	97	2.53	241.53	57.36
4964	-0.43	99	2.53	247.32	56.35
4964	-0.43	101	2.53	253.02	55.17
4964	-0.43	103	2.7	258.6	54.66
4964	-0.43	105	2.53	264.08	54.15
4964	-0.43	107	2.53	269.44	54.49
4964	-0.43	109	2.53	274.68	55.17
4964	-0.43	111	2.7	279.8	55.5

4964	-0.43	113	2.7	284.79	55.67
4964	-0.43	115	2.7	289.64	55.5
4964	-0.43	117	2.7	294.37	55.33
4964	-0.43	119	2.7	298.95	55.5
4964	-0.43	121	2.7	303.4	56.18
4964	-0.43	123	2.7	307.7	56.68
4964	-0.43	125	2.7	311.87	57.02
4964	-0.43	127	2.7	315.88	57.19
4964	-0.43	129	2.7	319.75	56.85
4964	-0.43	131	2.7	323.48	56.18
4964	-0.43	133	2.7	327.05	55.5
4964	-0.43	135	2.7	330.48	55.17
4964	-0.43	137	2.7	333.76	55.17
4964	-0.43	139	2.87	336.88	55.33
4964	-0.43	141	2.87	339.86	55.84
4964	-0.43	143	2.87	342.68	56.35
4964	-0.43	145	3.04	345.36	56.18
4964	-0.43	147	2.87	347.88	56.01
4964	-0.43	149	3.04	350.26	55.5
4964	-0.43	151	2.87	352.48	55
4964	-0.43	153	3.04	354.56	54.66
4964	-0.43	155	2.87	356.48	54.83
4964	-0.43	157	3.04	358.25	55.33
4964	-0.43	159	3.04	359.88	56.01
4964	-0.43	161	2.87	361.35	56.68
4964	-0.43	163	3.04	362.68	56.85
4964	-0.43	165	2.87	363.86	56.68
4964	-0.43	167	3.04	364.89	56.35
4964	-0.43	169	3.04	365.77	56.01
4964	-0.43	171	3.04	366.51	56.01

4964	-0.43	173	3.04	367.1	56.35
4964	-0.43	175	3.04	367.54	56.68
4964	-0.43	177	3.21	367.83	56.85
4964	-0.43	179	3.21	367.97	57.19
4964	-0.43	181	3.21	367.97	56.68
4964	-0.43	183	3.21	367.83	55.84
4964	-0.43	185	3.21	367.53	55.33
4964	-0.43	187	3.21	367.09	54.83
4964	-0.43	189	3.21	366.5	54.83
4964	-0.43	191	3.37	365.76	55.17
4964	-0.43	193	3.21	364.88	55.84
4964	-0.43	195	3.21	363.84	56.51
4964	-0.43	197	3.37	362.66	56.35
4964	-0.43	199	3.21	361.33	56.35
4964	-0.43	201	3.37	359.86	56.35
4964	-0.43	203	3.37	358.23	56.18
4964	-0.43	205	3.37	356.45	56.35
4964	-0.43	207	3.54	354.53	56.51
4964	-0.43	209	3.54	352.45	57.02
4964	-0.43	211	3.54	350.23	57.53
4964	-0.43	213	3.71	347.85	57.53
4964	-0.43	215	3.54	345.33	57.02
4964	-0.43	217	3.71	342.65	56.35
4964	-0.43	219	3.71	339.83	55.33
4964	-0.43	221	3.71	336.85	55.17
4964	-0.43	223	3.54	333.72	55.33
4964	-0.43	225	3.54	330.45	55.5
4964	-0.43	227	3.54	327.02	55.84
4964	-0.43	229	3.54	323.44	55.84
4964	-0.43	231	3.71	319.72	56.35

4964	-0.43	233	3.37	315.85	56.01
4964	-0.43	235	3.71	311.83	55.84
4964	-0.43	237	3.54	307.67	56.01
4964	-0.43	239	3.88	303.37	56.01
4964	-0.43	241	3.71	298.92	56.51
4964	-0.43	243	3.71	294.34	57.19
4964	-0.43	245	3.88	289.62	57.36
4964	-0.43	247	3.88	284.76	57.19
4964	-0.43	249	3.88	279.78	56.85
4964	-0.43	251	3.88	274.66	56.51
4964	-0.43	253	3.71	269.42	56.01
4964	-0.43	255	3.71	264.06	55.33
4964	-0.43	257	3.71	258.59	55.5
4964	-0.43	259	3.88	253	55.67
4964	-0.43	261	3.88	247.31	55.67
4964	-0.43	263	3.88	241.52	56.01
4964	-0.43	265	4.05	235.64	55.67
4964	-0.43	267	4.05	229.66	55.84
4964	-0.43	269	4.22	223.61	55.84
4964	-0.43	271	4.39	217.48	55.67
4964	-0.43	273	4.22	211.29	55.67
4964	-0.43	275	4.39	205.03	55.84
4964	-0.43	277	4.39	198.73	56.35
4964	-0.43	279	4.39	192.38	56.51
4964	-0.43	281	4.55	186	56.68
4964	-0.43	283	4.72	179.59	56.51
4964	-0.43	285	4.72	173.18	56.51
4964	-0.43	287	5.06	166.75	56.18
4964	-0.43	289	4.89	160.33	56.18
4964	-0.43	291	5.23	153.93	56.01

4964	-0.43	293	5.23	147.55	55.84
4964	-0.43	295	5.57	141.21	56.18
4964	-0.43	297	5.57	134.91	55.84
4964	-0.43	299	5.9	128.67	55.67
4964	-0.43	301	6.07	122.5	55.67
4964	-0.43	303	6.24	116.41	55.33
4964	-0.43	305	6.58	110.4	55.17
4964	-0.43	307	6.58	104.5	55.33
4964	-0.43	309	6.92	98.71	55.33
4964	-0.43	311	7.25	93.04	55.84
4964	-0.43	313	7.59	87.51	56.18
4964	-0.43	315	8.27	82.11	56.18
4964	-0.43	317	8.6	76.87	56.35
4964	-0.43	319	9.11	71.79	56.35
4964	-0.43	321	9.45	66.89	56.35
4964	-0.43	323	10.12	62.17	56.18
4964	-0.43	325	10.97	57.63	56.18
4964	-0.43	327	11.98	53.3	56.18
4964	-0.43	329	12.65	49.18	56.18
4964	-0.43	331	13.83	45.27	56.01
4964	-0.43	333	15.35	41.59	55.84
4964	-0.43	335	16.7	38.14	55.84
4964	-0.43	337	18.39	34.92	55.67
4964	-0.43	339	20.41	31.95	55.33
4964	-0.43	341	22.61	29.24	54.15
4964	-0.43	343	25.14	26.77	51.62
4964	-0.43	345	28.34	24.57	48.92
4964	-0.43	347	31.72	22.63	49.43
4964	-0.43	349	35.26	20.97	54.32
4964	-0.43	351	39.31	19.57	70.01

4964	-0.43	353	43.52	18.45	85.36
4964	-0.43	355	48.08	17.61	95.15
4964	-0.43	357	52.47	17.05	99.03
4964	-0.43	359	56.35	16.76	104.76
4964	-0.43	361	59.72	16.76	112.35
4964	-0.43	363	61.24	17.04	113.54
4964	-0.43	365	60.56	17.6	99.03
4964	-0.43	367	58.54	18.44	77.6
4964	-0.43	369	54.66	19.55	61.41
4964	-0.43	371	49.77	20.94	53.82
4964	-0.43	373	45.55	22.61	46.73
4964	-0.43	375	41.5	24.54	59.38
4964	-0.43	377	37.79	26.74	72.37
4964	-0.43	379	34.75	29.2	69.17
4964	-0.43	381	31.21	31.91	67.48
4964	-0.43	383	28.34	34.88	78.28
4964	-0.43	385	25.31	38.09	95.99
4964	-0.43	387	22.44	41.54	99.36
4964	-0.43	389	20.24	45.22	82.66
4964	-0.43	391	17.21	49.12	90.42
4964	-0.43	393	15.35	53.24	83.68
4964	-0.43	395	13.66	57.57	78.95
4964	-0.43	397	12.48	62.1	60.9
4964	-0.43	399	11.13	66.82	44.2
4964	-0.43	401	10.12	71.73	46.73
4964	-0.43	403	9.28	76.81	57.02
4964	-0.43	405	8.27	82.05	67.14
4964	-0.43	407	7.59	87.44	64.11
4964	-0.43	409	6.92	92.98	61.58
4964	-0.43	411	6.24	98.65	61.91

4964	-0.43	413	5.9	104.44	71.7
4964	-0.43	415	5.57	110.34	73.05
4964	-0.43	417	5.06	116.35	66.13
4964	-0.43	419	4.55	122.44	59.72
4964	-0.43	421	4.39	128.61	50.61
4964	-0.43	423	4.05	134.85	57.19
4964	-0.43	425	3.88	141.15	66.13
4964	-0.43	427	3.71	147.5	61.41
4964	-0.43	429	3.21	153.88	56.18
4964	-0.43	431	3.37	160.29	50.95
4964	-0.43	433	3.04	166.71	52.47
4964	-0.43	435	2.7	173.14	57.19
4964	-0.43	437	2.53	179.56	58.54
4964	-0.43	439	2.36	185.97	55.17
4964	-0.43	441	2.19	192.36	56.68
4964	-0.43	443	2.19	198.71	53.98
4964	-0.43	445	2.19	205.02	60.06
4964	-0.43	447	2.19	211.28	60.9
4964	-0.43	449	2.02	217.48	58.88
4964	-0.43	451	1.86	223.61	55.33
4964	-0.43	453	1.86	229.67	54.15
4964	-0.43	455	1.86	235.65	58.03
4964	-0.43	457	1.69	241.54	62.25
4964	-0.43	459	1.69	247.33	62.93
4964	-0.43	461	1.52	253.03	60.06
4964	-0.43	463	1.52	258.62	59.89
4964	-0.43	465	1.52	264.1	58.03
4964	-0.43	467	1.52	269.46	61.07
4964	-0.43	469	1.52	274.7	61.74
4964	-0.43	471	1.52	279.82	60.06

4964	-0.43	473	1.52	284.81	57.53
4964	-0.43	475	1.52	289.67	55.84
4964	-0.43	477	1.52	294.39	57.86
4964	-0.43	479	1.52	298.98	58.54
4964	-0.43	481	1.52	303.43	58.88
4964	-0.43	483	1.35	307.74	57.53
4964	-0.43	485	1.35	311.9	56.01
4964	-0.43	487	1.35	315.92	56.85
4964	-0.43	489	1.35	319.79	59.55
4964	-0.43	491	1.35	323.51	61.24
4964	-0.43	493	1.35	327.09	62.08
4964	-0.43	495	1.35	330.51	59.89
4964	-0.43	497	1.35	333.79	59.89
4964	-0.43	499	1.35	336.92	59.72
4964	-0.43	501	1.35	339.89	59.55
4964	-0.43	503	1.52	342.72	59.21
4964	-0.43	505	1.52	345.39	57.53
4964	-0.43	507	1.52	347.91	55.84
4964	-0.43	509	1.35	350.29	56.01
4964	-0.43	511	1.35	352.51	56.18
4964	-0.43	513	1.35	354.58	57.36
4964	-0.43	515	1.35	356.5	57.53
4964	-0.43	517	1.52	358.28	56.85
4964	-0.43	519	1.69	359.9	56.51
4964	-0.43	521	1.52	361.37	57.36
4964	-0.43	523	1.69	362.7	58.37
4964	-0.43	525	1.52	363.88	59.55
4964	-0.43	527	1.69	364.9	59.38
4964	-0.43	529	1.69	365.79	58.88
4964	-0.43	531	1.86	366.52	58.88

4964	-0.43	533	2.02	367.1	58.71
4964	-0.43	535	1.86	367.54	59.21
4964	-0.43	537	1.86	367.83	59.21
4964	-0.43	539	1.86	367.98	58.88
4964	-0.43	541	1.86	367.97	59.05
4964	-0.43	543	1.86	367.82	59.38
4964	-0.43	545	1.86	367.52	59.55
4964	-0.43	547	1.86	367.08	59.72
4964	-0.43	549	1.69	366.49	59.05
4964	-0.43	551	1.52	365.75	58.37
4964	-0.43	553	1.86	364.86	57.86
4964	-0.43	555	1.69	363.83	57.7
4964	-0.43	557	1.69	362.64	57.86
4964	-0.43	559	1.86	361.31	58.2
4964	-0.43	561	2.02	359.83	57.86
4964	-0.43	563	1.86	358.21	57.86
4964	-0.43	565	1.86	356.43	58.2
4964	-0.43	567	1.86	354.5	58.54
4964	-0.43	569	2.02	352.43	59.05
4964	-0.43	571	2.02	350.2	59.21
4964	-0.43	573	2.02	347.82	59.21
4964	-0.43	575	2.02	345.3	59.38
4964	-0.43	577	2.02	342.62	59.21
4964	-0.43	579	2.02	339.79	59.55
4964	-0.43	581	2.02	336.82	59.21
4964	-0.43	583	2.19	333.69	58.71
4964	-0.43	585	2.19	330.41	57.7
4964	-0.43	587	2.19	326.99	56.68
4964	-0.43	589	2.02	323.41	56.68
4964	-0.43	591	2.02	319.69	57.36

4964	-0.43	593	2.02	315.82	58.37
4964	-0.43	595	2.02	311.8	57.53
4964	-0.43	597	2.02	307.64	56.35
4964	-0.43	599	2.02	303.34	56.18
4964	-0.43	601	2.02	298.9	55.84
4964	-0.43	603	2.19	294.31	55.84
4964	-0.43	605	2.19	289.59	55.17
4964	-0.43	607	2.36	284.74	54.66
4964	-0.43	609	2.19	279.75	54.32
4964	-0.43	611	2.19	274.64	54.49
4964	-0.43	613	2.19	269.4	55.67
4964	-0.43	615	2.19	264.05	55.33
4964	-0.43	617	2.36	258.57	55.67
4964	-0.43	619	2.19	252.99	54.83
4964	-0.43	621	2.36	247.3	54.83
4964	-0.43	623	2.19	241.51	55.84
4964	-0.43	625	2.36	235.63	56.85
4964	-0.43	627	2.36	229.66	57.7
4964	-0.43	629	2.19	223.61	58.03
4964	-0.43	631	2.53	217.48	58.2
4964	-0.43	633	2.36	211.29	58.54
4964	-0.43	635	2.36	205.04	58.54
4964	-0.43	637	2.36	198.73	58.2
4964	-0.43	639	2.36	192.39	58.2
4964	-0.43	641	2.53	186.01	57.36
4964	-0.43	643	2.53	179.61	57.19
4964	-0.43	645	2.53	173.19	57.53
4964	-0.43	647	2.7	166.77	57.86
4964	-0.43	649	2.7	160.35	57.53
4964	-0.43	651	2.7	153.95	56.68

4964	-0.43	653	2.7	147.57	55.84
4964	-0.43	655	2.7	141.23	55.67
4964	-0.43	657	2.87	134.94	55.5
4964	-0.43	659	2.87	128.7	56.18
4964	-0.43	661	2.87	122.53	56.51
4964	-0.43	663	3.04	116.44	56.85
4964	-0.43	665	2.87	110.44	56.85
4964	-0.43	667	3.04	104.54	57.02
4964	-0.43	669	3.04	98.74	56.68
4964	-0.43	671	3.04	93.08	56.35
4964	-0.43	673	3.04	87.54	55.84
4964	-0.43	675	3.21	82.15	56.18
4964	-0.43	677	3.21	76.91	56.51
4964	-0.43	679	3.37	71.83	56.85
4964	-0.43	681	3.37	66.92	57.19
4964	-0.43	683	3.37	62.2	57.02
4964	-0.43	685	3.37	57.67	56.18
4964	-0.43	687	3.37	53.33	56.01
4964	-0.43	689	3.37	49.21	55.67
4964	-0.43	691	3.54	45.3	56.18
4964	-0.43	693	3.54	41.62	56.18
4964	-0.43	695	3.54	38.16	56.51
4964	-0.43	697	3.71	34.95	56.68
4964	-0.43	699	3.54	31.98	56.85
4964	-0.43	701	3.71	29.26	57.19
4964	-0.43	703	3.54	26.79	57.19
4964	-0.43	705	3.71	24.59	57.02
4964	-0.43	707	3.37	22.65	57.02
4964	-0.43	709	3.54	20.98	57.19
4964	-0.43	711	3.54	19.58	57.7

4964	-0.43	713	3.54	18.46	57.86
4964	-0.43	715	3.54	17.62	57.7
4964	-0.43	717	3.37	17.05	57.53
4964	-0.43	719	3.21	16.76	57.02

10. References

1. Athavale, S., Sajanpawar, P., 1991. Studies on some modelling aspects in the finite element analysis of small gasoline engine components. SAE Technical Paper.
2. Gopinath, D., Sushma, C.V., 2015. Design and Optimization of Four Wheeler Connecting Rod Using Finite Element Analysis. Materials Today: Proceedings 2, 2291-2299.
3. Hui, W., Chen, S., Zhang, Y., Shao, C., Dong, H., 2015. Effect of vanadium on the high-cycle fatigue fracture properties of medium-carbon microalloyed steel for fracture splitting connecting rod. Materials & Design 66, Part A, 227-234.
4. Park, H., Ko, Y.S., Jung, S.C., Song, B.T., Jun, Y.H., Lee, B.C., Lim, J.D., 2003. Development of fracture split steel connecting rods. SAE Technical Paper.
5. Repgen, B., 1998. Optimized connecting rods to enable higher engine performance and cost reduction. SAE Technical Paper.
6. Sarihan, V., Song, J.O., 1990. Optimization of the wrist pin end of an automobile engine connecting rod with an interference fit. Journal of Mechanical Design 112, 406-412.
7. Webster, W.D., Coffell, R., Alfaro, D., 1983. A three dimensional finite element analysis of a high speed diesel engine connecting rod. SAE Technical Paper.